

Feedback of superconducting fluctuations on charge order in the underdoped cupratesDebanjan Chowdhury¹ and Subir Sachdev^{1,2}¹*Department of Physics, Harvard University, Cambridge, Massachusetts 02138, USA*²*Perimeter Institute for Theoretical Physics, Waterloo, Ontario N2L 2Y5, Canada*

(Received 8 May 2014; revised manuscript received 7 October 2014; published 24 October 2014)

Metals interacting via short-range antiferromagnetic fluctuations are unstable to sign-changing superconductivity at low temperatures. For the cuprates, this leading instability leads to the well-known d -wave superconducting state. However, there is also a secondary instability to an incommensurate charge-density wave, with a predominantly d -wave form factor, arising from the same antiferromagnetic fluctuations. Recent experiments in the pseudogap regime of the hole-doped cuprates have found strong evidence for such a charge-density wave order and, in particular, the predicted d -wave form factor. However, the observed wave vector of the charge order differs from the leading instability in Hartree-Fock theory, and is that of a subleading instability. In this paper, we examine the feedback of superconducting fluctuations on these different charge-density wave states, and find that over at least a small temperature window, they prefer the experimentally observed wave vector.

DOI: [10.1103/PhysRevB.90.134516](https://doi.org/10.1103/PhysRevB.90.134516)

PACS number(s): 71.10.Hf, 75.10.Lp

I. INTRODUCTION

The pseudogap (PG) regime of the hole-doped cuprates is possibly one of the most enigmatic phases of matter. It has often been described as one of the central problems in the physics of high-temperature superconductivity (SC). It is identified by the onset of a large gap (~ 50 meV) below a temperature T^* , as observed in a number of different probes. The gap persists down to the superconducting transition temperature T_c , below which of course the system develops the usual superconducting gap. The nature of the fermionic excitations in the PG phase is particularly interesting—the aforementioned gap is present in the antinodal regions of the Brillouin zone close to momenta $(\pi, 0)$ and $(0, \pi)$; there exists, however, a region close to the nodes that remains gapless as has been detected via ARPES experiments [1,2]. These regions are commonly referred to as the Fermi “arcs.”

A topic of intense debate has been whether in addition to pairing fluctuations, any other possibly short-ranged and fluctuating phase with broken symmetry is also present above $T > T_c$, and below the onset of the pseudogap. Investigating the precise nature of this short-range order will likely shed some light on the “normal” state out of which it emerges. The different perspectives on this short-range order in the PG phase can be divided into two classes: (i) the order is “quantum disordered” and there are fractionalized excitations and associated topological excitations [3–6], or (ii) the order is “classically disordered” primarily due to thermal fluctuations. Here, we shall explore consequences arising from the second point of view. Implications of these thermal fluctuations on the phenomenology of the pseudogap phase, with comparison to various experiments, have also been explored recently [7,8].

A huge leap in our understanding came about with the discovery of quantum oscillations caused by a small electron-like pocket at very large magnetic fields [9]. This was the first clear evidence of the “normal” state in the pseudogap phase under large magnetic fields having some resemblance to a metallic state. More recently, in a series of remarkable experiments, it has become clear that the reconstructed electron-like pocket is caused by an incommensurate charge-density wave (CDW), competing with superconductivity [10–23]. The wave vector

of this charge-density wave, which is of the type $(\pm Q_0, 0)$, $(0, \pm Q_0)$, appears to be linked to the Fermi surface in the antinodal regions. Furthermore, diamagnetism measurements in YBCO show significant fluctuation diamagnetism over approximately the same range of temperatures where x-ray experiments measure charge order fluctuations, indicating that there are significant superconducting fluctuations in this phase [24,25]. A natural question that needs to be addressed is whether both SC and CDWs arise out of the same physics.

In the underdoped cuprates, due to the proximity to an antiferromagnet (AF) close to half filling, the susceptibility, $\chi(\mathbf{q})$, is peaked around $\mathbf{K} = \pm(\pi, \pi(1 - \delta))$, $\pm(\pi(1 - \delta), \pi)$ ($\delta \neq 0$ when the fluctuations are peaked around an incommensurate wave vector) [26]. It is now well understood that a metal interacting via such antiferromagnetic exchange interactions is unstable to d -wave superconductivity at low temperatures [27–29]. However, an interesting consequence of the AF exchange interactions is that they also give rise to a secondary instability to a charge-density wave with a predominantly d -wave form factor [30,31]. Significant recent developments have been the evidence for the predicted d -wave form factor in x-ray observations [21], and a direct phase-sensitive measurement of the d -wave form factor in scanning tunneling microscopy (STM) experiments [22]. In the present paper we will turn our attention to the wave vector of this CDW, and in particular, its connection to the SC fluctuations.

A number of recent works have addressed such issues [30–42]. In Refs. [30,31], the wave vector of the leading CDW instability has been found to be of the form $\pm(Q_0, Q_0)$, $\pm(Q_0, -Q_0)$, while the experimentally observed wave vector was a subleading instability. At this point it is useful to introduce some new notation. From now on, we shall often refer to the experimentally observed CDW with wave vectors $(Q_0, 0)$ and $(0, Q_0)$ as “CDW-a” and the one with wave vectors $(Q_0, \pm Q_0)$ as “CDW-b” (see Fig. 1). More recently, it has been pointed out that in the presence of strong correlations arising from on-site and nearest-neighbor Coulomb repulsion, it is possible to obtain a stable CDW-a phase, with the wave vectors seen in experiments, in a certain window of parameter space [37]. Wang and Chubukov [39] examined retardation

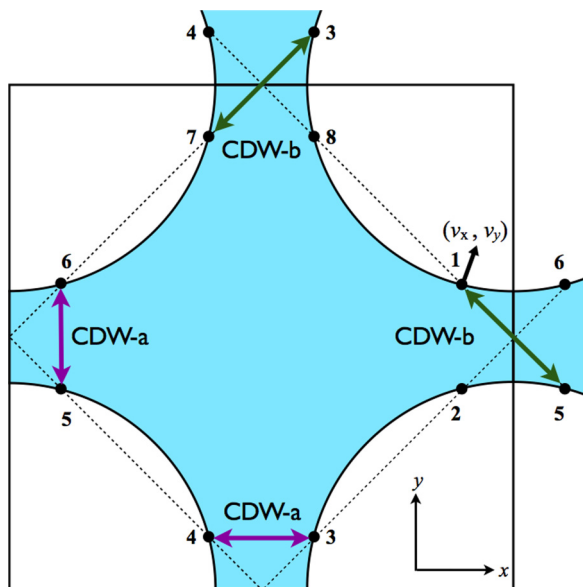


FIG. 1. (Color online) Generic Fermi surface for hole-doped cuprates, with the filled states shaded in blue. Solid circles, numbered 1, . . . , 8, represent hot spots where the Fermi surface intersects the magnetic Brillouin zone for a (π, π) SDW. The purple arrows represent the CDW-a wave vectors, which closely resemble the experimentally observed wave vector, while the green arrows represent the CDW-b wave vectors, which arise as the leading instability in a HF calculation. The Fermi velocity, (v_x, v_y) , is shown at the hot spot 1. The wave vectors of CDW-a are $(\pm Q_0, 0)$ and $(0, \pm Q_0)$, while those of CDW-b are $(Q_0, \pm Q_0)$. The computation in the present paper applies for a range of values of Q_0 , and not just when it is equal to the separation between hot spots as shown above; for different Q_0 we have to consider a corresponding set of 8 points around the Fermi surface, and our computations proceed unchanged.

effects linked to the damping of spin fluctuations with a long correlation length, and argued for an extension of CDW-a with time-reversal symmetry breaking. In this paper, we will show that upon accounting for the interplay between superconductivity and charge order in the underdoped cuprates, the CDW state with the correct wave vector (i.e., CDW-a) appears to be preferred over CDW-b over at least a small temperature window, as long as the antinodal regions of the Fermi surface are reasonably nested with a small curvature (a criterion to be made more precise later) [43]. In Fig. 1, Q_0 represents the separation between two neighboring “hot spots.” However, our computations in this paper are applicable for a range of different values of Q_0 that connect points in the antinodal regions and can be different from the hot-spot wave vector. Meier *et al.* [35] have also recently looked at the effect of superconducting fluctuations on charge order in a different setup.

We also note our recent work [6], which employs a quantum disordered model of the pseudogap as a topological metal, and proposes an alternative mechanism for charge ordering at the $(Q_0, 0)$, $(0, Q_0)$ wave vectors.

Our paper is organized as follows: In Sec. II A, we introduce the theory of a metal interacting via antiferromagnetic exchange interactions (henceforth referred to as t - J model, but without any on-site Coulomb repulsion) and review a

Hartree-Fock analysis for various charge-ordering and pair-density wave instabilities. Based on the leading instabilities that occur in a metal, we construct the minimal model in Sec. II B for a metal with pairing and charge-order fluctuations. In Sec. III, we take the low-energy limit of this theory and present the effective theory in the vicinity of special points—the “hot spots”—where the magnetic Brillouin zone corresponding to \mathbf{K} intersects the Fermi surface. We present the results of our computation, describing the mutual feedback of superconductivity and charge order on each other, in Secs. IV A and IV B. Finally in Sec. V, we summarize the main results emerging from this analysis. Some of the technical details are summarized in Appendices A and B.

II. MODEL

A. Metal with antiferromagnetic exchange interaction

In this section, we briefly review some of the earlier results [31] obtained by carrying out a Hartree-Fock (HF) analysis of the t - J model (without any Gutzwiller projection). Consider the following model for fermions, $c_{i\alpha}$, interacting via short-range antiferromagnetic exchange interactions,

$$H_{tJ} = \sum_{i,j} \left[(-t_{ij} - \mu \delta_{ij}) c_{i\alpha}^\dagger c_{j\alpha} + \frac{1}{2} J_{ij} \vec{S}_i \cdot \vec{S}_j \right], \quad (1)$$

where t_{ij} are the hopping amplitudes, μ denotes the chemical potential, J_{ij} are the AF exchange couplings, and $\vec{S}_i = c_{i\alpha}^\dagger \vec{\sigma}_{\alpha\beta} c_{i\beta} / 2$.

We are interested in looking at the various instabilities that can arise in this model in the particle-particle as well as particle-hole channel. We shall restrict our attention to pair-density wave (PDW), where the SC condensate carries a finite momentum, and charge-density wave states. We ignore the possibility of having spin order, partly motivated by most experiments on the non-La-based cuprates (e.g., YBCO and BSCCO), where the region of charge order has hardly any overlap with that of spin order [15]. For the Hartree-Fock analysis, we need the best variational estimate for the following mean-field Hamiltonian,

$$H_{MF} = \sum_{\mathbf{k}} \left[\varepsilon(\mathbf{k}) c_{\mathbf{k},\alpha}^\dagger c_{\mathbf{k},\alpha} + \sum_{\mathbf{Q}} \Delta_{\mathbf{Q}}(\mathbf{k}) \epsilon_{\alpha\beta} c_{-\mathbf{k}+\mathbf{Q}/2,\alpha} c_{\mathbf{k}+\mathbf{Q}/2,\beta} + \sum_{\mathbf{Q}} P_{\mathbf{Q}}(\mathbf{k}) c_{\mathbf{k}+\mathbf{Q}/2,\alpha}^\dagger c_{\mathbf{k}-\mathbf{Q}/2,\alpha} + \text{H.c.} \right]. \quad (2)$$

In the above, $\varepsilon(\mathbf{k})$ represents the electronic dispersion. All the functions $\Delta_{\mathbf{Q}}(\mathbf{k})$, $P_{\mathbf{Q}}(\mathbf{k})$ are variational parameters which will be optimized by minimizing the free energy, $F \leq F_{MF} + \langle H - H_{MF} \rangle_{MF}$. As mentioned earlier, we have allowed for a spin-singlet pair-density wave along with a charge-density wave at a finite wave vector, \mathbf{Q} . The pair-density wave at $\mathbf{Q} \rightarrow 0$ reduces to the standard BCS state where particles with opposite spins are paired at $\pm \mathbf{k}$.

Expanding the right-hand side of F in powers of $\Delta_Q(\mathbf{k})$ and $P_Q(\mathbf{k})$, we get

$$F = 2 \sum_{\mathbf{k}, \mathbf{k}', \mathbf{Q}} \Delta_Q^*(\mathbf{k}) \sqrt{\Pi_S(\mathbf{k})} \mathcal{M}_S(\mathbf{k}, \mathbf{k}') \sqrt{\Pi_S(\mathbf{k}')} \Delta_Q(\mathbf{k}') + \sum_{\mathbf{k}, \mathbf{k}', \mathbf{Q}} P_Q^*(\mathbf{k}) \sqrt{\Pi_C(\mathbf{k})} \mathcal{M}_C(\mathbf{k}, \mathbf{k}') \sqrt{\Pi_C(\mathbf{k}')} P_Q(\mathbf{k}'), \quad (3)$$

where the kernels $\mathcal{M}_{S,C}(\mathbf{k}, \mathbf{k}')$ are given by

$$\mathcal{M}_{S,C}(\mathbf{k}, \mathbf{k}') = \delta_{\mathbf{k}, \mathbf{k}'} + \frac{3}{V} \chi(\mathbf{k} - \mathbf{k}') \sqrt{\Pi_{S,C}(\mathbf{k}) \Pi_{S,C}(\mathbf{k}')}, \quad (4)$$

and the polarizabilities are

$$\Pi_S(\mathbf{k}) = \frac{1 - f(\varepsilon(\mathbf{k} + \mathbf{Q}/2)) - f(\varepsilon(-\mathbf{k} + \mathbf{Q}/2))}{\varepsilon(\mathbf{k} + \mathbf{Q}/2) + \varepsilon(-\mathbf{k} + \mathbf{Q}/2)}, \quad (5)$$

$$\Pi_C(\mathbf{k}) = \frac{f(\varepsilon(\mathbf{k} + \mathbf{Q}/2)) - f(\varepsilon(\mathbf{k} - \mathbf{Q}/2))}{\varepsilon(\mathbf{k} - \mathbf{Q}/2) - \varepsilon(\mathbf{k} + \mathbf{Q}/2)}, \quad (6)$$

with $f(\cdot)$ the Fermi function and $\chi(\mathbf{k}) (= \sum_{i,j} J_{ij} e^{i\mathbf{q} \cdot (\mathbf{r}_i - \mathbf{r}_j)} / 4)$ the AF susceptibility. Note that for dispersions that satisfy $\varepsilon(\mathbf{k} + \mathbf{Q}) = -\varepsilon(\mathbf{k})$, $\Pi_S(\mathbf{k}) = \Pi_C(\mathbf{k})$. This holds in the vicinity of the hot spots for certain values of \mathbf{Q} and will have important consequences, which we shall revisit later.

Pair-density wave and charge ordering in the metal occurs via condensation in the eigenmodes of the operators $\mathcal{M}_{S,C}$ with the lowest eigenvalues. In order to find the leading instability in the pairing and charge-ordering channel, we need to solve the following eigenvalue problem,

$$\frac{3}{V} \sum_{\mathbf{k}'} \sqrt{\Pi_S(\mathbf{k})} \chi(\mathbf{k} - \mathbf{k}') \sqrt{\Pi_S(\mathbf{k}')} \phi_S(\mathbf{k}') = \lambda_S \phi_S(\mathbf{k}'), \quad (7)$$

$$\frac{3}{V} \sum_{\mathbf{k}'} \sqrt{\Pi_C(\mathbf{k})} \chi(\mathbf{k} - \mathbf{k}') \sqrt{\Pi_C(\mathbf{k}')} \phi_C(\mathbf{k}') = \lambda_C \phi_C(\mathbf{k}'). \quad (8)$$

Instead of working with the form of $\chi(\mathbf{k})$ introduced above, we assume that the AF susceptibility, $\chi(\mathbf{q})$, has the form

$$\chi(\mathbf{q}) = \sum_{\mathbf{K}} \frac{\chi_0}{4\{\xi^{-2} + 2[2 - \cos(q_x - K_x) - \cos(q_y - K_y)]\}}, \quad (9)$$

which is peaked near the antiferromagnetic wave vector, \mathbf{K} (as introduced earlier), with ξ representing the AF correlation length and χ_0 the overall strength of the spin fluctuations. There is little difference between the results for $\delta = 0$ and $\delta \neq 0$.

In Figs. 2(a) and 2(b) we plot the lowest eigenvalues $\lambda_{S,C}/\chi_0$, obtained after diagonalizing Eq. (8) on a discrete Brillouin zone with L^2 points. We use the following electronic dispersion: $\varepsilon(\mathbf{k}) = -2t_1[\cos(k_x) + \cos(k_y)] - 4t_2 \cos(k_x) \cos(k_y) - 2t_3[\cos(2k_x) + \cos(2k_y)] - \mu$.

Let us start with a discussion of the pair-density wave state [Fig. 2(a)]. Not surprisingly, the state with $\mathbf{Q} = 0$ is the leading instability and in particular, $-\lambda_S$ for $\mathbf{Q} = 0$ has a logarithmic divergence as $T \rightarrow 0$. We do not find any other local minima in phase space; the BCS log for $\mathbf{Q} = 0$ simply overwhelms any other PDW state that might have otherwise arisen within this weak-coupling approach. Comparing the numerical values of the eigenvalues λ_S and λ_C in Figs. 2(a) and 2(b), it is clear that $-\lambda_S$ (at $\mathbf{Q} = 0$) is the smallest. Therefore, in the

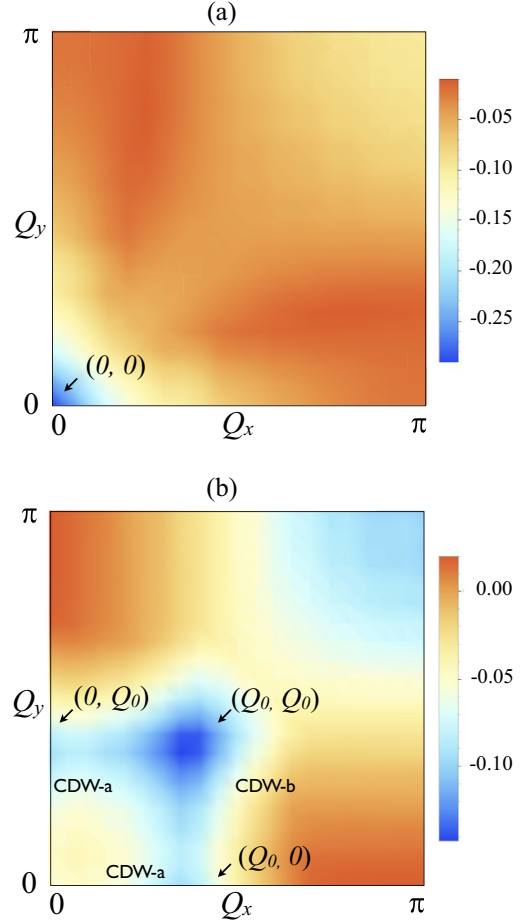


FIG. 2. (Color online) Plot of the smallest eigenvalue (a) λ_S/χ_0 and (b) λ_C/χ_0 as a function of Q_x and Q_y . We use a band structure with $t_1 = 1.0, t_2 = -0.32, t_3 = 0.128, \mu = -1.11856$ (corresponding to the same Fermi surface used in Ref. [31]). The other parameters are $\xi = 2, T = 0.1, \delta = 1/4$, and $L = 20$. For the pair-density wave, the global minimum is located at $\mathbf{Q} = 0$ while for the charge order, it is located at $\mathbf{Q} = (Q_0, Q_0)$ (CDW-b). In (b), note the “valleys” of local minima extending from (Q_0, Q_0) to $(Q_0, 0)$ and $(0, Q_0)$ (CDW-a)—the latter are local, but not global, minima.

presence of short-range AF interactions, the leading weak-coupling quadratic instability indeed turns out to be a SC (with d -wave symmetry; this information is contained in the structure of ϕ_S).

For the charge-ordering instability [Fig. 2(b)], the global minimum is located at the diagonal wave vector (Q_0, Q_0) . This corresponds to the CDW-b state introduced earlier. However notice the “valleys” of local minima extending from this wave vector to $(Q_0, 0)$ and $(0, Q_0)$, the CDW-a. It is also worth pointing out that the form factors associated with these CDWs, ϕ_C , primarily have a d -wave component. In real space, this implies that the charge-density modulation is mostly on the Cu-Cu links (bonds) rather than on the sites. Hence they are also referred to as bond-ordered states.

The reason why CDW-b turned out to be the leading CDW instability is actually related to two features in our problem above: (i) the absence of a gap in the spectrum at the antinodes, and (ii) an emergent particle-hole symmetry associated with the exchange interactions, $J_{ij} \vec{S}_i \cdot \vec{S}_j$. This exchange interaction

is invariant under independent SU(2) rotations on each lattice site that map particles to holes and vice versa. These rotations therefore naturally map SC to CDW-b. In the absence of any Fermi-surface curvature or other interaction terms that break this symmetry, both of these instabilities would be exactly degenerate. However, once it is broken, CDW-b becomes a subleading instability (SC is always guaranteed to remain the leading instability even in the presence of a curvature since the points $\pm\mathbf{k}$ are always “nested”; however, a very large nearest-neighbor Coulomb interaction term, Vn_in_j , can suppress superconductivity, for instance). We also note in passing that CDW-a is mapped to the PDW [44] at the same wave vector under these rotations; we do not consider this PDW here because it does not appear as a preferred eigenvalue of λ_S in Fig. 2(a).

The above analysis was carried out in the limit where the different orders were decoupled from each other; i.e., we did not look at the feedback of one over the other and analyzed the free energy F to only quadratic order. Let us therefore now construct a minimal model for SC and CDW fluctuations in a metal and analyze the effective theory beyond quadratic order in the next section.

B. Metal with SC and CDW fluctuations

Consider now a model for the fermions with a generic Fermi surface as shown in Fig. 1. Based on our HF analysis in the previous section, we know the (sub)leading instabilities were to a (i) d -wave superconductor, (ii) CDW-b with wave vectors $(Q_0, \pm Q_0)$, and (iii) CDW-a with wave vectors $(Q_0, 0)$ and $(0, Q_0)$. We can use this information to construct a model for a metal with strong pairing and CDW fluctuations. Therefore, we consider the theory for the fermions coupled to superconducting (Ψ) and CDW (Φ) fluctuations (which are in their uncondensed phase, as is the case in the PG regime). The Hamiltonian is then given by

$$H = H_0 + H_S + H_B, \quad (10)$$

where

$$H_0 = \sum_{\mathbf{k}} (\varepsilon_{\mathbf{k}} - \mu) c_{\mathbf{k},\alpha}^\dagger c_{\mathbf{k},\alpha}, \quad (11)$$

$$H_S = \sum_{\mathbf{k}} [\Delta_s(\mathbf{k}) c_{\mathbf{k}+\mathbf{q}/2,\uparrow}^\dagger c_{-\mathbf{k}+\mathbf{q}/2,\downarrow}^\dagger \Psi_{\mathbf{q}} + \text{H.c.}], \quad (12)$$

$$H_B = \sum_{\mathbf{k},\mathbf{q}} \left[\left(\sum_{\mathbf{Q}} P_{\mathbf{Q}}(\mathbf{k}) \Phi_{\mathbf{q}-\mathbf{Q}} \right) c_{\mathbf{k}+\mathbf{q}/2,\alpha}^\dagger c_{\mathbf{k}-\mathbf{q}/2,\alpha} + \text{H.c.} \right]. \quad (13)$$

In the above, $\Delta_s(\mathbf{k})$ is the usual form factor associated with d -wave superconductivity and $P_{\mathbf{Q}}(\mathbf{k})$ is the form factor for CDW with wave vector \mathbf{Q} . We would now like to obtain an effective action in terms of Ψ and Φ (both CDW-a and CDW-b) after integrating out the fermions. The aim of this work is to study the effect of SC fluctuations on these two different CDW states and to analyze whether the competition between the different order parameters can preferentially select a particular state. It will be particularly interesting if this state corresponds to the one that has been seen experimentally.

III. LOW-ENERGY THEORY

Instead of carrying out the above task with the full Fermi surface, let us analyze the theory in the vicinity of the hot spots labeled $j = 1, \dots, 8$ in Fig. 1. We expand the dispersion close to the hot spots so that

$$\varepsilon_{\mathbf{k},j} = v_{F,\mathbf{k}_j} k_{\perp} + \kappa k_{\parallel}^2, \quad (14)$$

with k_{\perp} (k_{\parallel}) being the momentum normal (parallel) to the Fermi surface. The Fermi velocities are given by $\mathbf{v}_{F,\mathbf{k}_1} = (v_x, v_y)$, $\mathbf{v}_{F,\mathbf{k}_2} = (v_x, -v_y)$, $\mathbf{v}_{F,\mathbf{k}_4} = (-v_y, -v_x)$, and $\mathbf{v}_{F,\mathbf{k}_7} = (-v_y, v_x)$. The other velocities can be obtained similarly by symmetry. The parameter κ is related to the Fermi surface curvature.

The bare Lagrangian for the fermions in the vicinity of the hot spots, ψ_j ($j = 1, \dots, 8$), is then given by

$$\mathcal{L}_0 = \sum_{j=1}^8 [\psi_j^\dagger (i\omega - \varepsilon_{\mathbf{k},j}) \psi_j]. \quad (15)$$

The same expansion can be carried out for a set of any eight points in the antinodal regions, that are not necessarily connected by the hot-spot wave vectors.

A. Form factor of the CDW

There are two fundamental properties associated with the CDW orders—the wave vector and the structure of the form factor. We have explored the wave vectors that can arise in our HF computation in Sec. II A, while the form factors associated with the different CDW orders for the full underlying Fermi surface were already computed in Ref. [31]. In this section, we shall revisit this issue within our low-energy formulation.

If we go back to Eq. (3) and focus only on the terms involving charge order, we obtain

$$F_C = \sum_{\mathbf{Q}} \left[\sum_{\mathbf{k}} |P_{\mathbf{Q}}(\mathbf{k})|^2 \Pi_C(\mathbf{k}) + \frac{3}{V} \sum_{\mathbf{k},\mathbf{k}'} \chi(\mathbf{k} - \mathbf{k}') \Pi_C(\mathbf{k}) \Pi_C(\mathbf{k}') P_{\mathbf{Q}}^*(\mathbf{k}) P_{\mathbf{Q}}(\mathbf{k}') \right]. \quad (16)$$

We now assume that $\chi(\mathbf{k} - \mathbf{k}')$ is peaked at $\mathbf{k} - \mathbf{k}' = \mathbf{K} = (\pi, \pi)$ and perform the integrations over \mathbf{k} and \mathbf{k}' in patches in the neighborhoods of the hot spots that satisfy the above constraint. Furthermore, we assume that $P_{\mathbf{Q}}(\mathbf{k})$ can be treated as piecewise constant in the patches and treat χ as static and noncritical; i.e., $\chi \approx \chi_0/\xi^{-2}$. For CDW-b, let us focus on the hot-spot pairs {2,6} and {7,3} where $P_{\mathbf{Q}}(\mathbf{k})$ takes the values Υ_1^b and Υ_2^b . Similarly, for CDW-a, we choose to focus on the pairs {1,2} and {4,7} where $P_{\mathbf{Q}}(\mathbf{k})$ takes the values Υ_1^a and Υ_2^a .

It is straightforward to see that for CDW-b, $\Pi_C(\mathbf{k})$ evaluated in the patches {2,6} and {7,3} are equal to each other due to purely geometric reasons, i.e., $\Pi_1^b = \Pi_2^b = \Pi^b$, so that

$$F_C|_b = \Pi^b [|\Upsilon_1^b|^2 + |\Upsilon_2^b|^2] + \frac{3\chi_0}{\xi^{-2}} (\Pi^b)^2 [\Upsilon_1^{b*} \Upsilon_2^b + \Upsilon_2^{b*} \Upsilon_1^b]. \quad (17)$$

It is simple to diagonalize the above quadratic form and obtain the optimum linear combination of Υ_1^b and Υ_2^b . For CDW-b,

the eigenvector corresponding to the lower eigenvalue has a purely d -wave form.

We can now do the same computation for CDW-a and we immediately find that $\Pi_1^a \neq \Pi_2^a$ (once again, for purely geometric reasons), so that

$$F_C|_a = \Pi_1^a |\Upsilon_1^a|^2 + \Pi_2^a |\Upsilon_2^a|^2 + \frac{3\chi_0}{\xi^{-2}} \Pi_1^a \Pi_2^a [\Upsilon_1^{a*} \Upsilon_2^a + \Upsilon_2^{a*} \Upsilon_1^a]. \quad (18)$$

We can diagonalize the above quadratic form and find that the eigenvector corresponding to the lower eigenvalue contains a mixture of d - and s -wave forms. It is important to note that there is an ambiguity in choosing the eigenvector of the quadratic form [31,38]: we can rescale $\Upsilon_1^a, \Upsilon_2^a$ by different factors (i.e., perform a similarity transform) before diagonalizing the quadratic form, and then undo the similarity transform after the diagonalization. This modifies the eigenvectors except when the lowest eigenvalue is zero. It was argued [31,38] that the appropriate similarity transform is determined by looking at the structure of the particle-hole T matrix, which leads to the requirement that the diagonal terms in the quadratic form have equal values. In this manner, we find that the eigenvector with lower eigenvalue has $(\Upsilon_1^a, \Upsilon_2^a) \propto (1/\sqrt{\Pi_1^a}, -1/\sqrt{\Pi_2^a})$.

In order to estimate the difference between Π_1^a and Π_2^a , we can do an explicit computation at $T = 0$ and in the absence of a Fermi-surface curvature, so that

$$\Pi_1^a = \frac{2}{4\pi^2 v_x v_y} \int_{-\Lambda_x}^{\Lambda_x} dx \int_0^{\Lambda_y} dy \frac{\theta(y-x) - \theta(-y-x)}{2y}, \quad (19)$$

where $\Lambda_{x,y} = v_{x,y} \Lambda$, $\theta(\cdot)$ represents the Heaviside step function, and we are integrating near the hot spots in a momentum window $|\mathbf{k}| < \Lambda$, with Λ a UV regulator. We are interested in the limit $\Lambda_y > \Lambda_x$ (since $v_y > v_x$ in the antinodal regions) and obtain

$$\Pi_1^a = \frac{\Lambda}{2\pi^2 v_y} \left[1 + \ln \left(\frac{v_y}{v_x} \right) \right]. \quad (20)$$

On the other hand,

$$\Pi_2^a = \frac{2}{4\pi^2 v_x v_y} \int_0^{\Lambda_x} dx \int_{-\Lambda_y}^{\Lambda_y} dy \frac{\theta(y+x) - \theta(y-x)}{2x}, \quad (21)$$

$$\Pi_2^a = \frac{\Lambda}{2\pi^2 v_y}. \quad (22)$$

Therefore, we see that

$$\Pi_1^a = \eta \Pi_2^a > 0, \quad (23)$$

where

$$\eta = 1 + \ln(v_y/v_x). \quad (24)$$

We then conclude from the discussion below Eq. (18) that the ratio of the s to the remaining bond components in the form factor of CDW-a is

$$\left| \frac{\Upsilon_1^a + \Upsilon_2^a}{\Upsilon_1^a - \Upsilon_2^a} \right| = \frac{\sqrt{\eta} - 1}{\sqrt{\eta} + 1}, \quad (25)$$

which can be quite small. We expect the aforementioned remaining component of the CDW to be d . (Although the present hot-spot computation does not, strictly speaking,

distinguish between s' and d , demanding smooth variation of the form factor in the antinodal region strongly prefers d).

Wang and Chubukov [39] also analyzed the form factor of CDW-a by looking at the set of coupled CDW vertices, retaining the Landau damping terms in the bosonic propagator. (In particular our $\eta \rightarrow 1$ limit corresponds to $\varphi \rightarrow \pi/4$ in their notation.)

B. Interplay of charge-order and superconductivity

In Sec. II A, we saw that at quadratic order one does not obtain the CDW with the experimentally measured wave vector. Therefore, it is necessary to go to quartic order; our real interest in this section is to compute these terms and, in particular, their temperature dependencies.

Let us now write the full low-energy theory in terms of the (a) fermions, ψ_j , (b) CDW-a (Φ_x^a, Φ_y^a) with wave vectors $\mathbf{Q}_x^a = (Q_0, 0)$ and $\mathbf{Q}_y^a = (0, Q_0)$, (c) CDW-b (Φ_x^b, Φ_y^b) with wave vectors $\mathbf{Q}_x^b = (Q_0, Q_0)$ and $\mathbf{Q}_y^b = (Q_0, -Q_0)$, and (d) SC (Ψ):

$$\mathcal{L} = \mathcal{L}_0 + \mathcal{L}_S + \mathcal{L}_B, \quad (26)$$

$$\mathcal{L}_S = \Psi(\psi_1^\dagger \psi_5^\dagger + \psi_2^\dagger \psi_6^\dagger) - \Psi(\psi_7^\dagger \psi_3^\dagger + \psi_4^\dagger \psi_8^\dagger) + \text{H.c.}, \quad (27)$$

$$\begin{aligned} \mathcal{L}_B = & \Phi_x^a(\psi_6^\dagger \psi_1 + \psi_5^\dagger \psi_2 - \psi_3^\dagger \psi_4 - \psi_8^\dagger \psi_7) \\ & - \Phi_y^a(\psi_1^\dagger \psi_2 + \psi_6^\dagger \psi_5 - \psi_3^\dagger \psi_8 - \psi_4^\dagger \psi_7) \\ & + \Phi_x^b(\psi_6^\dagger \psi_2 - \psi_3^\dagger \psi_7) - \Phi_y^b(\psi_5^\dagger \psi_1 - \psi_8^\dagger \psi_4) + \text{H.c.}, \end{aligned} \quad (28)$$

where we have suppressed the momentum and spin-index structure above and \mathcal{L}_0 was already expressed in Eq. (15). While writing \mathcal{L}_B , we have ignored the possibility of having a small s -wave component in the form factors of $\Phi_{x,y}^a$; i.e., we have assumed $P_Q(\mathbf{k}) = \cos k_x - \cos k_y$. We also choose not to write any explicit coupling constants as they can be absorbed into the fields by a redefinition. In the low-energy limit, the patches 1-2-5-6 and 3-4-7-8 are decoupled from each other.

Once again, we integrate out the fermions in the vicinity of the hot spots (in a momentum window $|\mathbf{k}| < \Lambda$) and compute the action up to fourth order in Φ^a, Φ^b , and Ψ . All the four-point diagrams contributing to these terms are shown in Fig. 3. There is also a three-point diagram, as shown in Fig. 4, contributing to the effective action, which takes the form

$$\begin{aligned} S_{\text{eff}}[\Phi^a, \Phi^b, \Psi] = & \int d^2\mathbf{r} d\tau [r_a (|\Phi_x^a|^2 + |\Phi_y^a|^2) + r_b (|\Phi_x^b|^2 + |\Phi_y^b|^2) \\ & + r_b |\Psi|^2 + u_a (|\Phi_x^a|^4 + |\Phi_y^a|^4) + u_b (|\Phi_x^b|^4 + |\Phi_y^b|^4) \\ & + u_b |\Psi|^4 + u_{ab} (|\Phi_x^a|^2 + |\Phi_y^a|^2) (|\Phi_x^b|^2 + |\Phi_y^b|^2) \\ & + w_a |\Phi_x^a|^2 |\Phi_y^a|^2 \\ & + \bar{u}_{ab} ((\Phi_x^a)^2 \Phi_x^{b*} \Phi_y^{b*} + (\Phi_y^a)^2 \Phi_x^{b*} \Phi_y^b + \text{H.c.}) \\ & + t_{ab} (\Phi_x^a \Phi_y^a \Phi_x^{b*} + \Phi_x^a \Phi_y^{a*} \Phi_y^{b*} + \text{H.c.}) \\ & + s_a |\Psi|^2 (|\Phi_x^a|^2 + |\Phi_y^a|^2) + s_b |\Psi|^2 (|\Phi_x^b|^2 + |\Phi_y^b|^2)], \end{aligned} \quad (29)$$

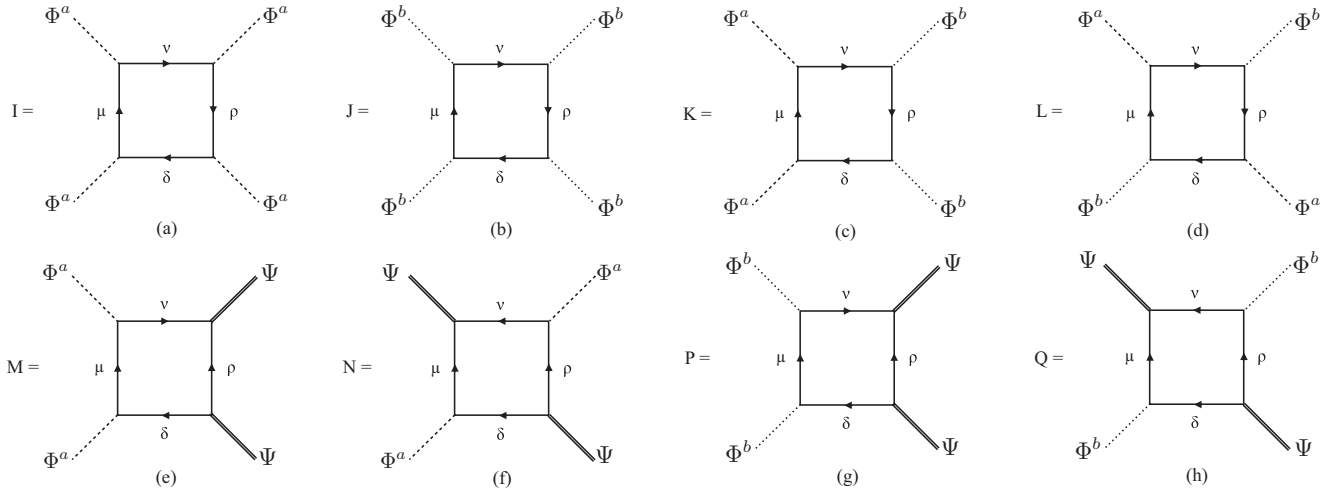


FIG. 3. Feynman diagrams representing the various 4-point functions that contribute to different terms in S_{eff} . The solid internal lines carry different hot-spot indices (μ, ν, ρ, δ) depending on the term being evaluated. The dashed, dotted, and double lines represent Φ^a , Φ^b , and Ψ , respectively. The individual diagrams are labeled (a) $I_{\mu\nu\rho\delta}$, (b) $J_{\mu\nu\rho\delta}$, (c) $K_{\mu\nu\rho\delta}$, (d) $L_{\mu\nu\rho\delta}$, (e) $M_{\mu\nu\rho\delta}$, (f) $N_{\mu\nu\rho\delta}$, (g) $P_{\mu\nu\rho\delta}$, (h) $Q_{\mu\nu\rho\delta}$.

where $r_a = a(T - T_{c,0}^a)$ and $r_b = b(T - T_{c,0}^b)$ with $a, b > 0$ and the bare transition temperatures, $T_{c,0}^b > T_{c,0}^a$. Note that we have already utilized the emergent symmetry of the linearized hot-spot theory to equate the transition temperatures for SC and CDW-b, and also equated the coefficients of $|\Psi|^4$ and $|\Phi_x^b|^4, |\Phi_y^b|^4$. In the presence of terms that break this symmetry, $T_{c,0}^b < T_{c,0}^a$; the exact details are beyond the scope of this work.

It is important to note that the above action is invariant under all the underlying symmetries (including under rotations; e.g., $\mathcal{R}_{\pi/2} : \Phi_x^a \rightarrow \Phi_y^a, \Phi_y^a \rightarrow \Phi_x^{a*}, \Phi_x^b \rightarrow \Phi_y^{b*}, \Phi_y^b \rightarrow \Phi_x^b$). The terms in the third and fourth lines arise naturally due to the existence of two types of CDW correlations in the system with wave vectors that satisfy the following geometric constraints: $\mathbf{Q}_x^b = \mathbf{Q}_x^a + \mathbf{Q}_y^a$ and $\mathbf{Q}_y^b = \mathbf{Q}_x^a - \mathbf{Q}_y^a$. Some of these coefficients were computed for the full Fermi surface in Ref. [40]. Note the absence of a term of the form $|\Phi_x^b|^2 |\Phi_y^b|^2$ above, which is allowed by symmetry but missing due to lack of available phase space for this kind of a scattering process. The terms that are of particular interest to us appear in the last line ($\sim s_a, s_b$), as will become clear in the next section. Let us now present the results for the different coefficients that appear above.

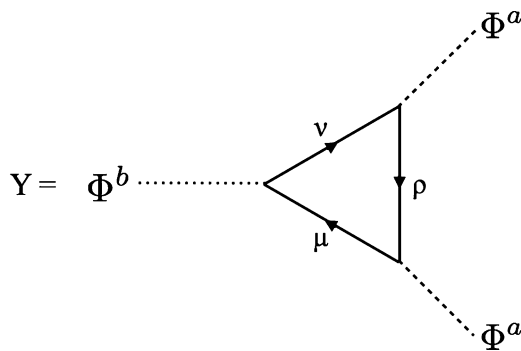


FIG. 4. Feynman diagram representing the 3-point function, $Y_{\mu\nu\rho}$, between Φ^a (dashed lines) and Φ^b (dotted line). The solid internal lines carry different hot-spot indices (μ, ν, ρ).

IV. RESULTS

We start by presenting the results for the linearized theory (i.e., set $\kappa = 0$) in the vicinity of the hot spots.

A. Linearized hot-spot theory

In this section, we shall list the expressions for the coefficients in terms of the loop integrals. The details of the computation are presented in Appendix A. At the outset, we note the regime that we are working in here—we assume that $T \ll v_x \Lambda \ll v_y \Lambda$; i.e., the temperature is much lower than any other ultraviolet energy scale in the problem and furthermore, the regions in the vicinity of the hot spots (and in the antinodal regions) are almost nested. In the next section, we will show that the Fermi-surface curvature, κ , introduces another temperature scale in the problem above which our analysis remains valid.

We start with u_a , representing the coefficient of the $|\Phi_x^a|^4, |\Phi_y^a|^4$ term [Fig. 3(a)]. Evaluating the contributions arising from both the patches, we obtain

$$u_a = -(I_{1616} + I_{2525} + I_{3434} + I_{7878}) \quad (30)$$

$$= -(I_{1212} + I_{3838} + I_{4747} + I_{5656}), \quad (31)$$

where it is straightforward to see that $I_{1616} = I_{2525} = I_{3838} = I_{4747}$, and $I_{1212} = I_{3434} = I_{5656} = I_{7878}$. The loop integrals are given by

$$I_{1212} = -\frac{1}{2} \int_{\mathbf{k}} G_1^2 G_2^2 \approx -\frac{1}{16\pi^2 v_x^2 v_y \Lambda} \frac{1}{(1 + (\frac{\pi T}{v_x \Lambda})^2)}, \quad (32)$$

$$I_{2525} = -\frac{1}{2} \int_{\mathbf{k}} G_2^2 G_5^2 = 0, \quad (33)$$

where we use the notation $\int_{\mathbf{k}} \equiv T \sum_m \int dk_x dk_y / (2\pi)^2$ and all the internal Green's functions carry the same argument: $(i\omega_m, \mathbf{k})$, with $\omega_m = (2m + 1)\pi T$. Note that in the limit of $T \ll v_x \Lambda$, $I_{1212} \rightarrow -1/(16\pi^2 v_x^2 v_y \Lambda)$; i.e., it is nonsingular and approaches a constant independent of temperature.

The competition term between Φ_x^a and Φ_y^a , described by w_a [also, Fig. 3(a)], is given by

$$w_a = -(2S + V), \quad (34)$$

where

$$S = I_{2565} + I_{5212} + I_{2161} + I_{1656}, \quad (35)$$

$$V = 4I_{1256}. \quad (36)$$

In the above, S, V represent the self-energy and vertex-correction type diagrams. Furthermore, it is straightforward to see that $I_{2565} = I_{5212} = I_{2161} = I_{1656}$. The explicit expressions are given by

$$I_{2565} = - \int_{\mathbf{k}} G_2 G_5^2 G_6 \approx - \frac{1}{8\pi^2 v_x^2 v_y \Lambda} \ln \left(\frac{v_x \Lambda}{\pi T} \right), \quad (37)$$

$$I_{1256} = - \int_{\mathbf{k}} G_1 G_2 G_5 G_6 = - \frac{1}{32 v_x v_y T}, \quad (38)$$

where the second integral has been evaluated in the limit $v_x \Lambda \rightarrow \infty$. Therefore, we see that the most singular contribution to w_a comes from I_{1256} and is $\sim 1/T$. This has interesting consequences, as will be discussed at the end of this section, and has also been pointed out by a recent work [39].

Similarly, the contributions to the $|\Phi^b|^4$ terms arise from [Fig. 3(b)]

$$u_b = -(J_{2626} + J_{3737}) = -(J_{1515} + J_{4848}), \quad (39)$$

where due to the underlying symmetries, all the diagrams turn out to be equal; i.e., $J_{1515} = J_{2626} = J_{3737} = J_{4848}$. The integral evaluates to

$$J_{1515} = - \frac{1}{2} \int_{\mathbf{k}} G_1^2 G_5^2 = - \frac{7\zeta(3)}{32\pi^4} \frac{\Lambda}{v_y T^2}, \quad (40)$$

where $\zeta(n)$ is the Riemann-zeta function. The singularity here is much stronger than what we encountered before in the case of the $|\Phi^a|^4$ terms. However, the T^{-2} behavior is not at all surprising—recall that there is a perfect $SU(2)$ symmetry between CDW-b and SC within our linearized theory and the coefficient of the $|\Phi^b|^4$ term should therefore be identical to that of $|\Psi|^4$, which is known to be of the same T^{-2} form. In the presence of a finite curvature, this symmetry will be broken below some temperature scale set by κ , as we shall see in the next section.

Let us now shift our focus to terms that describe the competition between the different components of the charge orders, Φ^a and Φ^b . There are two types of four-point functions between these orders, denoted u_{ab} and \bar{u}_{ab} . Let us focus on u_{ab} first [Fig. 3(c)]. If we focus only on the coefficient of, let us say, the $|\Phi_x^a|^2 |\Phi_x^b|^2$ term (the overall form in which the different order parameters appear is strongly constrained by various symmetries), we get

$$u_{ab} = -2(K_{1626} + K_{4373}), \quad (41)$$

where $K_{4373} = K_{6515}$ by symmetry under $\mathcal{R}_{\pi/2}$ (and the latter appears in the coefficient of $|\Phi_y^a|^2 |\Phi_y^b|^2$). Evaluating these loop

integrals gives

$$K_{1626} = - \int_{\mathbf{k}} G_1 G_2 G_6^2 = - \frac{1}{64 v_x v_y T}, \quad (42)$$

$$K_{6515} = - \int_{\mathbf{k}} G_1 G_5^2 G_6 = - \frac{1}{64 v_x v_y T}. \quad (43)$$

Similarly, while evaluating \bar{u}_{ab} [Fig. 3(d)], if we focus only on the coefficient of $(\Phi_x^a)^2 \Phi_x^{b*} \Phi_y^{b*}$ (the overall form of the terms is once again constrained by symmetry),

$$\bar{u}_{ab} = -(L_{2516} + L_{3784}), \quad (44)$$

where $L_{3784} = L_{2516}$ and the explicit form is given by

$$L_{2516} = - \int_{\mathbf{k}} G_1 G_2 G_5 G_6 = - \frac{1}{32 v_x v_y T}. \quad (45)$$

It is interesting to note that the leading singularities in all of the above diagrams (with the exception of u_a, u_b) are of the form $\sim 1/T$. This is something that we can understand by applying standard power-counting arguments. In $(2+1)$ -dimensions for such 4-point functions, the singular structure in the IR (with a cutoff, $k_0 \sim T$) will be obtained as $\int d^3k/k^4 \sim 1/k_0$, where $k \equiv (i\omega, \mathbf{k})$. However, there are obviously exceptions to this naive argument, which arise due to the interesting pole structure of the propagators involved in the different diagrams.

We now move over to the terms that actually describe the competition between CDW and SC—these will be responsible for some of the interesting results to come out of our analysis. We start by evaluating the diagrams contributing to s_a , which describes competition between Φ^a and Ψ [Figs. 3(e), 3(f)],

$$s_a = 2\bar{S} + \bar{V}, \quad (46)$$

where

$$\begin{aligned} \bar{S} &= M_{2515} + M_{6151} + M_{7848} + M_{4373} \\ &= M_{1262} + M_{6515} + M_{8373} + M_{4737}, \end{aligned} \quad (47)$$

$$\bar{V} = N_{2615} + N_{8437} = N_{2651} + N_{8473}. \quad (48)$$

In the above, \bar{S} and \bar{V} represent the self-energy and vertex correction contributions, respectively. We have written the coefficients of both $|\Phi_x^a|^2 |\Psi|^2$ and $|\Phi_y^a|^2 |\Psi|^2$ above, which are of course equal. Moreover, some of the symmetry-related diagrams are individually equal as well, such as $M_{1262} = M_{7848} = M_{6515} = M_{4373}$ and $M_{2515} = M_{8373} = M_{4737} = M_{6151}$. Similarly, $N_{2651} = N_{2615} = N_{8437} = N_{8473}$. The explicit expressions for the (distinct) diagrams are given by

$$M_{2515} = - \int_{\mathbf{k}} G_2 G_5^2 G_1' = \frac{1}{64 v_x v_y T}, \quad (49)$$

$$M_{1262} = - \int_{\mathbf{k}} G_1 G_2^2 G_6' = \frac{1}{64 v_x v_y T}, \quad (50)$$

$$N_{2651} = - \int_{\mathbf{k}} G_1 G_2 G_5' G_6' = - \frac{1}{32 v_x v_y T}. \quad (51)$$

The ‘‘primed’’ Green’s functions have arguments $(-i\omega_m, -\mathbf{k})$. Once again, the leading singularity is of the form $1/T$.

Finally, the coefficient s_b , which describes the competition between Φ^b and Ψ [Figs. 3(g) and 3(h)] is given by

$$s_b = 2(P_{2626} + P_{3737}) + (Q_{2626} + Q_{3737}) \quad (52)$$

$$= 2(P_{1515} + P_{4848}) + (Q_{1515} + Q_{4848}), \quad (53)$$

where all the self-energy type diagrams, $P_{1515} = P_{2626} = P_{3737} = P_{4848}$, are equal and the vertex-correction type diagrams are equal and opposite in sign to the self-energy type ones; i.e., $Q_{1515} = Q_{2626} = Q_{3737} = Q_{4848} = -P_{1515}$. We therefore only need to evaluate one such integral—the corresponding expression is given by

$$P_{2626} = - \int_{\mathbf{k}} G_2 G_6^2 G_2' = \frac{7\zeta(3)}{16\pi^4} \frac{\Lambda}{v_y T^2}. \quad (54)$$

The $1/T^2$ behavior is to be expected by the same reasoning that was presented earlier—the coefficients of $|\Psi|^4$, $|\Phi^b|^4$ and $|\Phi^b|^2|\Psi|^2$ should have an identical (singular) structure arising from the emergent SU(2) symmetry.

Now that we have evaluated all the four-point functions allowed by symmetry, let us also evaluate the three-point functions between Φ^a, Φ^b that contribute to t_{ab} (Fig. 4). Once again, we remind the reader that such a term is allowed because of purely geometric reasons associated with the wave vectors of the various CDWs: $\mathbf{Q}_x^b = \mathbf{Q}_x^a + \mathbf{Q}_y^a$ and $\mathbf{Q}_y^b = \mathbf{Q}_x^a - \mathbf{Q}_y^a$. If we focus on the coefficient of the $\sim \Phi_x^a \Phi_y^a \Phi_x^{b*}$ term (and the rest just follows by symmetry), we get

$$t_{ab} = (Y_{261} + Y_{265} + Y_{374} + Y_{378}), \quad (55)$$

where it is easy to see that $Y_{265} = Y_{261} = Y_{374} = Y_{378}$. If we choose to evaluate just one of these,

$$Y_{261} = - \int_{\mathbf{k}} G_1 G_2 G_6 = 0. \quad (56)$$

It is very interesting to see that within our linearized theory, the integral evaluates exactly to 0. However, in the presence of a finite curvature, this term assumes a nonzero value, as will be shown in the next section.

Assembling all the expressions that we have computed above, the leading (singular) behavior of the coefficients in the effective action, $S_{\text{eff}}[\Phi^a, \Phi^b, \Psi]$, are given by

$$u_a = \frac{1}{8\pi^2 v_x^2 v_y \Lambda}, \quad w_a = \frac{1}{8v_x v_y T}, \quad u_b = \frac{7\zeta(3)\Lambda}{16\pi^4 v_y T^2}, \quad (57)$$

$$u_{ab} = \frac{1}{16v_x v_y T}, \quad \bar{u}_{ab} = \frac{1}{16v_x v_y T}, \quad t_{ab} = 0, \quad (58)$$

$$s_a = \frac{1}{16v_x v_y T}, \quad s_b = \frac{7\zeta(3)\Lambda}{8\pi^4 v_y T^2}. \quad (59)$$

At this point, it is worth pointing out some of the interesting features associated with the above terms. First of all, notice that depending on the nature of the term, we have obtained two different types of singularities—there are terms that go as $1/T$, and others that go as $1/T^2$ —in addition to the nonsingular term. This has two interesting consequences. In the presence of only the terms involving CDW-a, the competition between the x, y components, w_a , far exceeds u_a ; i.e., $w_a/u_a \sim \Lambda v_x/T \gg 1$. The implication is that at low enough temperatures, CDW-a would necessarily have a tendency to form stripelike, instead of checkerboard, order [39], which would spontaneously break

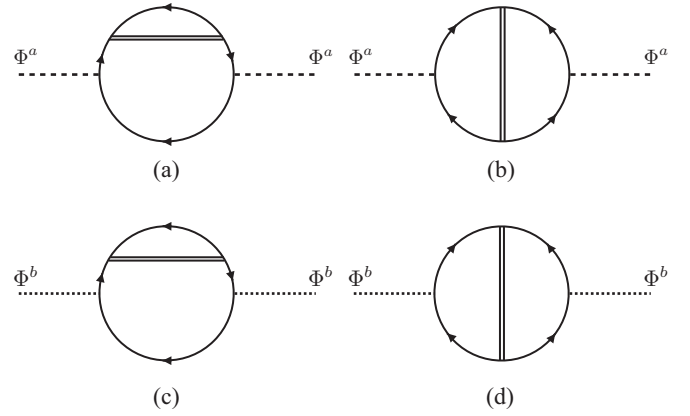


FIG. 5. Contracting the Ψ fields (solid double lines) in (a) $M_{\mu\nu\rho\delta}$, (b) $N_{\mu\nu\rho\delta}$ renormalize the $|\Phi^a|^2$ term, and (c) $P_{\mu\nu\rho\delta}$, (d) $Q_{\mu\nu\rho\delta}$ renormalize the $|\Phi^b|^2$ term.

the underlying C_4 symmetry of the lattice. On the other hand, with only CDW-b order, due to the absence of any competition between its x, y components, there will not be any tendency to break the C_4 symmetry. There is indication for the CDW being unidirectional and stripelike in the absence of a magnetic field in various experiments.

Let us now discuss an important feature of our analysis, involving the s_a, s_b terms that describe the competition of the different CDWs with SC. We find that $s_b/s_a \sim \Lambda v_x/T \gg 1$, implying that at low enough temperatures, SC competes with CDW-b much more strongly than with CDW-a. However, this is not surprising for the following reason: In our linearized hot-spot theory, there is no fundamental difference between CDW-b and SC due to the SU(2) symmetry. In fact both of these orders are strongly coupled to each other and compete for density of states on the Fermi surface in the vicinity of the same hot spots. Therefore, it is natural for them to compete with each other more strongly. The same is not true about CDW-a and SC, which compete for density of states along different portions of the Fermi surface. Note that CDW-a and CDW-b also compete mutually, so suppressing one naturally makes it favorable for the other one to emerge.

To summarize, the results of this section indicate that at very high temperatures, there is an almost perfect symmetry between CDW-b and SC (in fact, this symmetry persists even in the presence of a finite curvature, as we shall show in the next section), which makes it unfavorable for CDW-a to appear in the scene. However, as a function of decreasing temperature, as the strength of superconducting fluctuations increase, the CDW-b fluctuations are preferentially suppressed compared to CDW-a, which could possibly allow CDW-a to emerge. The exact crossovers, if any, are beyond the scope of this work. The net effect of the SC fluctuations is to effectively renormalize the quadratic terms in the action for Φ^a and Φ^b , as shown in Fig. 5. At low temperatures, the coefficient of $|\Phi^b|^2$ is renormalized more strongly compared to the coefficient of $|\Phi^a|^2$. In order to extract an estimate of the relative renormalizations, let us compute Δr_a and Δr_b for CDW-a,b due to purely thermal and Gaussian fluctuations associated with superconductivity, $\langle |\Psi_{\mathbf{q}}|^2 \rangle \sim (\mathbf{q}^2 + \sigma^2)^{-1}$. This approximation is valid sufficiently far away from the superconducting

T_c . The renormalizations are then given by

$$\begin{aligned}\Delta r_a &\approx s_a \int \frac{d^2q}{(2\pi)^2} \frac{1}{q^2 + \sigma^2} \approx -\frac{s_a}{2\pi} \ln\left(\frac{\sigma}{\Lambda}\right) \\ &= -\frac{1}{32\pi v_x v_y T} \ln\left(\frac{\sigma}{\Lambda}\right),\end{aligned}\quad (60)$$

$$\begin{aligned}\Delta r_b &\approx s_b \int \frac{d^2q}{(2\pi)^2} \frac{1}{q^2 + \sigma^2} \approx -\frac{s_b}{2\pi} \ln\left(\frac{\sigma}{\Lambda}\right) \\ &= -\frac{7\zeta(3)\Lambda}{16\pi^5 v_y T^2} \ln\left(\frac{\sigma}{\Lambda}\right).\end{aligned}\quad (61)$$

Hence, the relative renormalizations $\Delta r_b/\Delta r_a \sim \Lambda v_x/T \gg 1$, which indicates that within our simplified theory, there exists an intermediate range of temperatures where the transition temperature for CDW-b gets suppressed more than the one for CDW-a.

The only caveat in the calculations presented in this section is that all of them were performed in the limit of $\kappa \rightarrow 0$. Of course, in the actual problem, the curvature is finite (albeit small, in the antinodal region). Therefore, we revisit the whole problem with a nonzero curvature in the next section and analyze the consequences numerically.

We would like to remind the reader that at the level of approximation that we have used in this section, the CDW-a state is degenerate with the corresponding PDW state and the two compete strongly with each other. However, in the presence of a curvature or other features that break the SU(2) symmetry, the PDW state is destroyed completely, at least within the weak-coupling picture (unlike the other states, as we saw in Fig. 2). Moreover, as we shall see in the next section, the competition effects between CDW-a,b and SC discussed above survive even in the presence of curvature as long as the temperature is higher than a scale set by κ .

B. Effect of Fermi-surface curvature

In the previous section we ignored the effect of the Fermi-surface curvature completely and analyzed the linearized theory in the vicinity of the hot spots. Most of the graphs that we evaluated were singular in the limit of $T \rightarrow 0$ (though we intend to apply our results to the metallic state at strictly $T > 0$). The question we would now like to address is, to what extent do these results remain valid and what is the regime of validity, in the presence of a finite curvature. In fact, it is possible that the curvature sets a temperature scale above which our analytical results for the linearized theory continue to hold. We shall denote all the previously evaluated integrals by $\tilde{I}, \tilde{J}, \dots, \tilde{Q}, \tilde{Y}$, to distinguish them from the symbols used earlier. This time around, we shall perform the Matsubara sums first and then evaluate the momentum integrals numerically as a function of temperature for various fixed values of curvature, κ , and $\alpha = v_y/v_x$.

The aim of this computation is twofold. First of all, in the limit of $\kappa \rightarrow 0$, we should recover the temperature dependencies of the different terms obtained earlier. Second, we would like to have an approximate estimate of the functional form of $T_0(\kappa, \alpha)$, the temperature scale above which our analytical results for the $\kappa = 0$ problem continue to hold, assuming such a scale exists.

In the presence of a finite curvature, the modified dispersions are now given by

$$\varepsilon_1(\mathbf{k}) = v_x k_x + v_y k_y + \kappa(k_x^2 + k_y^2), \quad (62)$$

$$\varepsilon_2(\mathbf{k}) = v_x k_x - v_y k_y + \kappa(k_x^2 + k_y^2), \quad (63)$$

with $\varepsilon_5(\mathbf{k}) = \varepsilon_1(-\mathbf{k})$, $\varepsilon_6(\mathbf{k}) = \varepsilon_2(-\mathbf{k})$, and so on.

We only present the main findings of this analysis in the present section. The technical details of the computations along with plots of the numerical results are provided in Appendix B.

Let us start by analyzing the temperature dependence of diagrams (\tilde{I}_{1212}) contributing to u_a . We found that (i) at a fixed value of α , but for $\kappa \neq 0$, \tilde{I}_{1212} goes to a constant value in the limit of $T \rightarrow 0$. Moreover, in the limit of $\kappa \rightarrow 0$, this constant is nearly identical to what we had computed earlier for I_{1212} [Eq. (33)]. (ii) On the other hand, for $T \rightarrow v_x \Lambda$, there is a power-law fall-off going as $\sim 1/T^2$ for all considered values of κ , which again matches with our analytical result for I_{1212} [Eq. (33)]. (iii) Finally, \tilde{I}_{1212} scales as $\sim 1/\alpha$, which was apparent from the perfect scaling collapse that we observed for $\alpha \tilde{I}_{1212}$ (not shown). This agrees with our analytical results from earlier, even though they were computed with $\kappa = 0$. The numerically evaluated results for \tilde{I}_{1212} are shown in Fig. 6(a).

We next computed the leading diagrams contributing to w_a , giving rise to competition between x and y components of CDW-a. We came across the following interesting results: (i) irrespective of the value of the curvature, the diagrams all asymptote to a $1/T$ behavior at low temperatures (up to $T/v_x \Lambda \sim 10^{-4}$). (ii) There were however deviations at higher temperatures. (iii) Finally, this particular diagram also scales as $1/\alpha$ (not shown). The plots as a function of temperature are shown in Fig. 6(b).

It is especially interesting to see that even in the presence of a small curvature, w_a continues to scale as $1/T$ down to very low temperatures. However, as a function of decreasing temperature, there will be a preemptive instability to superconductivity, which in turn will cut off the $1/T$ behavior to $1/\Delta$, where Δ is the superconducting gap.

Let us now revisit the terms that turned out to be the most singular in our earlier analysis, which includes u_b (J_{1515}) and s_b (P_{2626}, Q_{2626}), and went as $\sim 1/T^2$. As a reminder, in the linearized theory, we obtained $2J_{1515} = -P_{2626} = Q_{2626}$. However, a finite curvature breaks this symmetry. We first focused on the temperature dependence of these diagrams at a fixed α but different values of κ and noticed the following common features: (i) The limit of $\kappa \rightarrow 0$ computation agrees perfectly with the analytical computation from the previous section. (ii) With an increasing κ , we note that the results for the different computations (i.e., with and without κ) only agree with each other above a characteristic temperature, $T_0 = C\kappa$, with C different for each diagram (this is determined by noting the temperature, T_0 , at which the deviation starts; these are marked by the dotted vertical lines in Fig. 7). To investigate whether C is α dependent, we computed the same diagrams as a function of temperature at a fixed $\kappa \neq 0$ and v_x , but for different values of α . Remarkably, the value of T_0 remains unaffected by changing α , which shows that C is independent of α . (iii) We also observed them to scale as $\sim 1/\alpha$, just like in all the previous cases. Therefore, to summarize, u_b and s_b

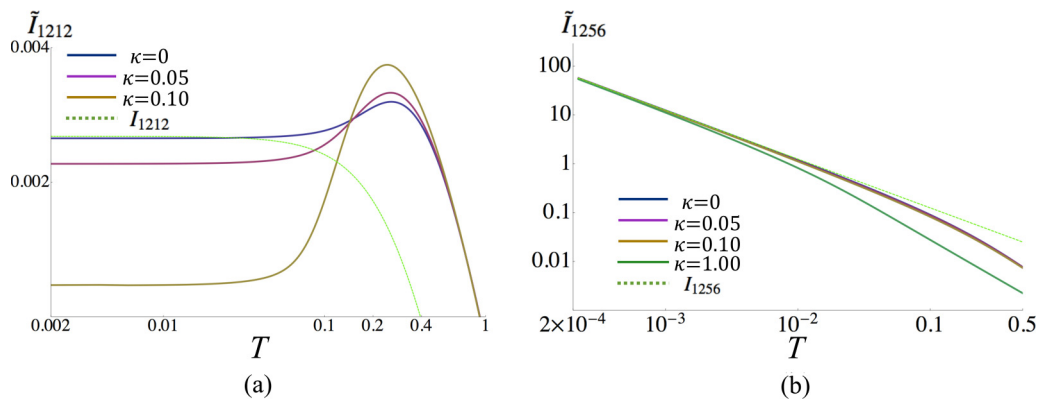


FIG. 6. (Color online) Absolute values of diagrams contributing to u_a and w_a as a function of temperature T for (a), (b) different values of κ but fixed $\alpha = 10.0$. Other parameters are $\Lambda = 2.0$ and $v_x = 0.5$. Note the almost perfect agreement of the analytical result for $\kappa = 0$ (dashed green line) with the numerical results for small curvature at low temperatures.

continue to behave as $1/T^2$ above a temperature scale that is set by curvature, $T_0 \sim \kappa$. Therefore, at high enough temperatures compared to this scale, the degeneracy between CDW-b and SC is maintained and the competition is sufficiently weak that it is unlikely that CDW-a will be a preferred state, based on our arguments from the previous section. It is however important to remind ourselves that the coefficient of $|\Psi|^4$, which also goes as $\sim 1/T^2$, survives even in the presence of a finite curvature but is eventually cut off by Δ . The numerically evaluated results are shown as a function of temperature in Figs. 7(a)–7(f).

Finally, we also evaluated the term responsible for competition between SC and CDW-a. Recall that in the linearized theory, $2M_{2515} = -N_{2651} = -N_{2615}$ and where the leading singularities were all $\sim 1/T$. However, in the presence of a finite κ these degeneracies are lifted. However, all the diagrams continue to behave as $\sim 1/T$ down to temperatures of $T/v_x\Lambda \sim 10^{-4}$, even in the presence of a reasonably large κ . However, as a function of decreasing temperature, the system will go superconducting thereby cutting off the singularity. We have also checked that just like all the other diagrams considered so far, these

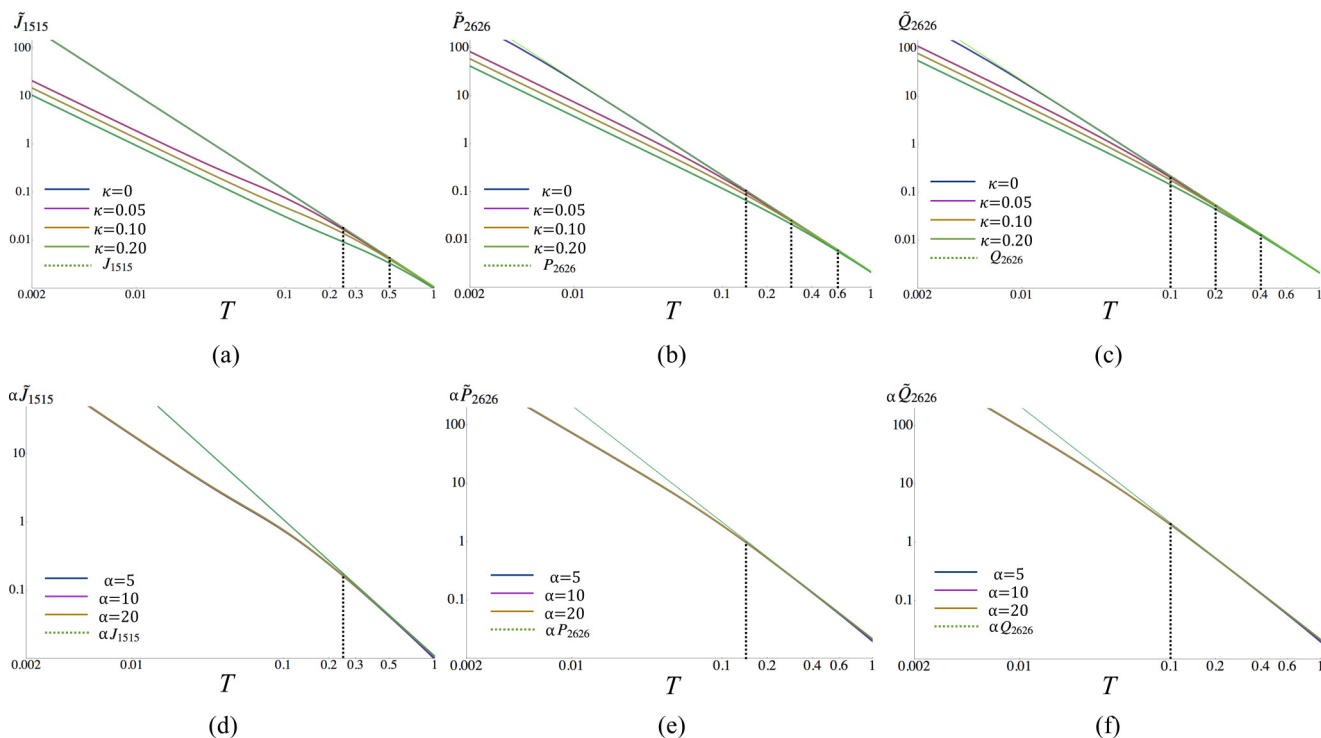


FIG. 7. (Color online) Absolute values of diagrams contributing to u_b and s_b as a function of temperature T for (a)–(c) different values of κ but fixed $\alpha = 10.0$ and (d)–(f) different values of α but fixed $\kappa = 0.05$. (a) \tilde{J}_{1515} , (b) \tilde{P}_{2626} , (c) \tilde{Q}_{2626} . (d)–(f) plot the same diagrams scaled with α . Other parameters are $\Lambda = 2.0$ and $v_x = 0.5$. The vertical black dotted lines represent the approximate temperature where the computation in the presence of a nonzero κ starts deviating from the one with $\kappa = 0$. Note that in panels (a)–(c), the green dashed curves (representing the analytical results) overlap almost perfectly with the blue solid curves for $\kappa = 0$.

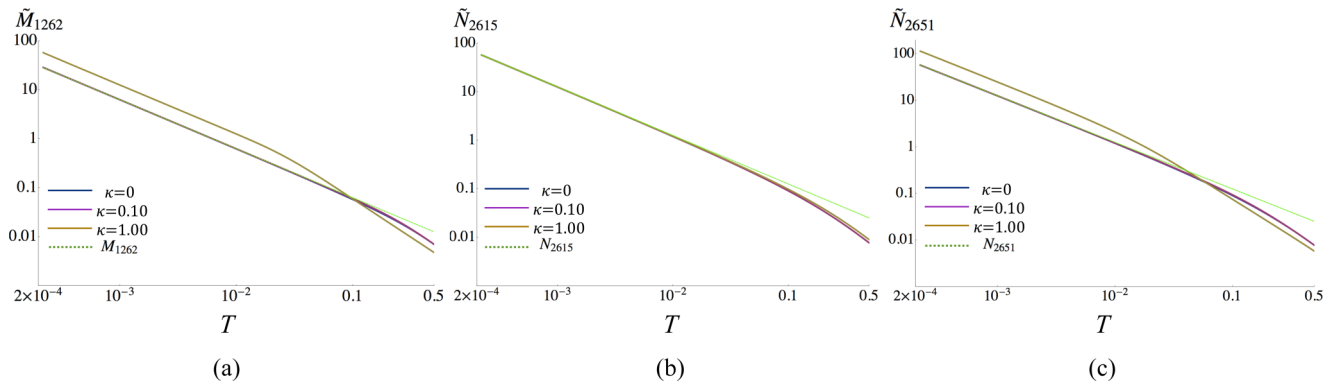


FIG. 8. (Color online) Absolute values of diagrams contributing to s_a as a function of temperature T for (a) \tilde{M}_{1262} , (b) \tilde{N}_{2615} , (c) \tilde{N}_{2651} for different values of κ but fixed $\alpha = 10.0$. Other parameters are $\Lambda = 2.0$ and $v_x = 0.5$. Note the almost perfect agreement of the analytical result for $\kappa = 0$ (dashed green line) with the numerical results for small curvature at low temperatures.

diagrams also scale as $\sim 1/\alpha$. The results are shown in Figs. 8(a)–8(c).

Towards the end of Sec. IV A, we saw that the three-point functions between CDW-a and CDW-b turned out to be identically zero. However, when we evaluated the same diagrams in the presence of a finite curvature, they turned out to be nonzero. In fact, based on the numerically evaluated results, we were able to guess an analytical functional form for \tilde{Y}_{261} , which is as follows,

$$\mathcal{Y}(T, \kappa, \alpha) \approx \frac{\kappa \Lambda}{\pi^2 \alpha v_x} \frac{1}{\pi^2 T^2 + v_x^2 \Lambda^2}. \quad (64)$$

Note that it indeed reproduces the $\kappa \rightarrow 0$ limit correctly and approaches a constant in the limit of $T \rightarrow 0$ otherwise. The numerically evaluated results and a comparison with \mathcal{Y} are shown in Figs. 9(a) and 9(b).

To conclude this section, we found that at sufficiently high temperatures, our results from the previous section continue to hold even in the presence of a finite, but small, curvature. The terms that we found to be most singular in our earlier computation ($\sim 1/T^2$) continue to have the same form as long as $T > T_0 \sim C\kappa$. On the other hand, the terms that went as $\sim 1/T$ continue to do so down to very low temperatures compared to the scales set by the Fermi velocities. However, as a function of decreasing temperature, these singularities are cut off eventually by the preemptive

instability to superconductivity. It is therefore safe to conclude that our computations in Sec. IV A are applicable in the window $\max\{T_c, T_0\} < T < v_x \Lambda \ll v_y \Lambda$.

V. DISCUSSION

Over the past few years, we have learned a great deal about the nature of the various symmetry-broken states that arise in the pseudogap regime of the underdoped cuprates. This has largely been possible due to the enormous number of remarkable experiments performed on these materials. Most of these experiments point toward the existence of a fluctuating and short-ranged charge-density wave in a metallic state; the onset of the CDW happens below a characteristic scale $T_{\text{cdw}} \lesssim T^*$, as deduced from x-ray scattering measurements [7]. There is a considerable amount of evidence suggesting that the CDW competes with superconductivity. It is therefore essential to understand the true nature of the CDW and its relation to superconductivity, as this might be the key to gaining a complete understanding of the pseudogap phase out of which both orders emerge [8].

Theoretically, we have now started to realize that the cuprates are a model system where the Fermi surface geometry, the strong interactions between the constituent electrons and the quasi-two-dimensional structure conspire to give rise to some remarkable consequences. One of these is the universal feature that in the presence of strong antiferromagnetic

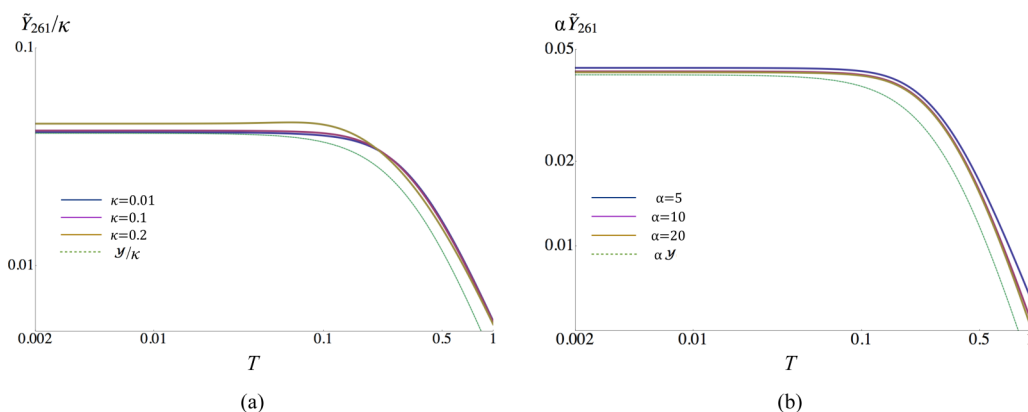


FIG. 9. (Color online) Absolute value of \tilde{Y}_{261} as a function of temperature and comparison with \mathcal{Y} (a) at fixed $\alpha = 10$, (b) at fixed $\kappa = 0.1$.

interactions, superconductivity and charge order are tied to each other; this has been highlighted by the observation [21,22] of the predicted [30,31] d -wave form factor of the CDW. While SC and CDW necessarily arise as dual instabilities of the same normal state, they also compete with each other. One of the puzzling features, on the theoretical side, has been the discrepancy between the wave vector of the CDW seen experimentally and the one obtained from the leading CDW instabilities in various models. The primary purpose of this paper has been to address one interesting ingredient that could be partly responsible for resolving this discrepancy over at least an intermediate window of temperature. The primary motivation for invoking the effect of d -wave superconducting fluctuations was to suppress density of states in the antinodal regions.

In this work, we studied the interplay of fluctuating charge order and superconductivity. Our starting point was the t - J model (without Gutzwiller projection) for a metal interacting via short-range antiferromagnetic exchange interactions, where the various instabilities at the Hartree-Fock level are to SC and CDWs with different sets of wave vectors (a t - J - V model with an infinite on-site Hubbard U also leads to similar instabilities, in addition to a staggered flux state [37]). The leading CDW-b state was found to have a wave vector of the form $\pm(Q_0, \pm Q_0)$, while there was a subleading instability to the CDW-a with wave vectors $(\pm Q_0, 0)$ and $(0, \pm Q_0)$. It is the latter that is closely related to the state seen in the experiments. In order to study the minimal model with all the necessary ingredients, we then considered the theory of a metal with pairing fluctuations and both types of CDW correlations and computed the effective Ginzburg-Landau (GL) theory up to the quartic order in the low-energy limit.

We obtained a number of interesting results for the temperature dependencies of the coefficients in the GL theory. In particular, one of the central results of this paper is the nature of the competition between CDW-a and CDW-b with SC. We observed that SC competes with CDW-b much more strongly than with CDW-a at low enough, but nonzero, temperatures. In the low-energy limit, we attributed this to the emergent SU(2) symmetry between SC and CDW-b, which really does not distinguish between the two different phases, and the absence of a gap in the spectrum at the antinodes. At low temperatures, we presented hints that the SC fluctuations might make it more favorable for CDW-a to arise and CDW-b to be suppressed

preferentially. In fact, we showed that even in the presence of a finite Fermi-surface curvature, the results for the mutual competition between CDW-a,b and SC continue to hold above a temperature scale that is set by the curvature ($T_0 \sim \kappa$). However at the same time, it is important to note that in the $\kappa \rightarrow 0$ limit, CDW-a is related by SU(2) symmetry to the PDW state with the same wave vectors and these two orders would therefore compete strongly with each other. However when the SU(2) symmetry is broken explicitly by a finite Fermi-surface curvature (or by a nearest-neighbor Coulomb repulsion term), the fragile PDW state disappears completely, as witnessed in our HF computation for the t - J model. It would be interesting to explore the interplay between SC, CDW, and PDW orders beyond weak coupling, starting from a microscopic model in the near future.

Finally, if it is indeed the superconducting fluctuations that are responsible for giving rise to the experimentally observed wave vector, then it is possible that the CDW-b state would show up in experiments if one were to suppress these SC fluctuations completely. Furthermore, the CDW-b order should have a tendency to form checkerboard order, unlike CDW-a, which has a tendency to form stripelike order [39,45]. This is a direction worth exploring in STM experiments at very high magnetic fields, for instance, and repeating phase-resolved analysis similar to what has been carried out recently to look for signatures of the CDW-a state [22]. However, if the CDW-b state continues to be absent, then it is likely that there are other factors at play here in addition to the SC fluctuations. One such factor has already been considered recently, which arises from strong correlation effects due to Coulomb repulsion [37].

ACKNOWLEDGMENTS

We thank A. Allais, J. Bauer, E. Berg, F. Laliberté, J. Lee, M. Metlitski, M. Norman, M. Punk, J. Sau, L. Taillefer, Y. Wang, and especially A. Chubukov for helpful discussions. D.C. thanks the Weizmann Institute for hospitality, where a part of this work was done. The research was supported by the U.S. National Science Foundation under Grant No. DMR-1103860, and by the Templeton Foundation. This research was also supported in part by Perimeter Institute for Theoretical Physics; research at Perimeter Institute is supported by the Government of Canada through Industry Canada and by the Province of Ontario through the Ministry of Research and Innovation.

APPENDIX A: FEYNMAN DIAGRAMS FOR LINEARIZED HOT-SPOT THEORY

In this Appendix, we provide details of the calculations for some of the loop integrals evaluated earlier. The momentum integrals will all be done with a cutoff Λ , since we only want to restrict ourselves to the neighborhood of the hot spots. We start with the diagrams that contribute to u_a ,

$$I_{2525} = -\frac{T}{2} \sum_m \int_{|\mathbf{k}| < \Lambda} \frac{1}{[i\omega_m - (v_x k_x - v_y k_y)]^2} \frac{1}{[i\omega_m - (-v_x k_x - v_y k_y)]^2}, \quad (\text{A1})$$

$$I_{1212} = -\frac{T}{2} \sum_m \int_{|\mathbf{k}| < \Lambda} \frac{1}{[i\omega_m - (v_x k_x + v_y k_y)]^2} \frac{1}{[i\omega_m - (v_x k_x - v_y k_y)]^2}. \quad (\text{A2})$$

It is useful to change the coordinates to $x = v_x k_x$, $y = v_y k_y$ so that $\Lambda_{x,y} = \Lambda v_{x,y}$. We are in the regime where $\Lambda_y \gg \Lambda_x \gg T$. The above integrals then become

$$I_{2525} = -\frac{T}{8\pi^2 v_x v_y} \sum_m \int_{-\Lambda_x}^{\Lambda_x} dx \int_{-\Lambda_y}^{\Lambda_y} dy \frac{1}{(i\omega_m - x + y)^2} \frac{1}{(i\omega_m + x + y)^2}, \quad (\text{A3})$$

$$I_{1212} = -\frac{T}{8\pi^2 v_x v_y} \sum_m \int_{-\Lambda_x}^{\Lambda_x} dx \int_{-\Lambda_y}^{\Lambda_y} dy \frac{1}{(i\omega_m - x - y)^2} \frac{1}{(i\omega_m - x + y)^2}. \quad (\text{A4})$$

We shall always evaluate the k_y integral first and use $\int_{-\Lambda_y}^{\Lambda_y} dk_y = \int_{-\infty}^{\infty} dk_y - \int_{|k_y| > \Lambda_y} dk_y = \mathcal{I}_1 - \mathcal{I}_2$.

The contribution to I_{2525} from \mathcal{I}_1 , i.e., $I_{2525}|_1 = 0$ (poles on same side). From \mathcal{I}_2 , we get

$$I_{2525} \Big|_2 \approx \frac{T \Lambda_x}{4\pi^2 v_x v_y} \sum_m \int_{\Lambda_y}^{\infty} dy \left[\frac{1}{(y + i\omega_m)^4} + \frac{1}{(y - i\omega_m)^4} \right] = 0. \quad (\text{A5})$$

Therefore, we have $I_{2525} = 0$. For I_{1212} , we get

$$\begin{aligned} I_{1212} \Big|_1 &= -\frac{iT}{16\pi v_x v_y} \sum_m \text{sgn}(\omega_m) \int_{-\Lambda_x}^{\Lambda_x} \frac{dx}{(x - i\omega_m)^3} = -\frac{T}{8\pi v_x v_y} \int_{-\Lambda_x}^{\Lambda_x} dx \sum_{m>0} \frac{\omega_m^3 - 3x^2 \omega_m}{(\omega_m^2 + x^2)^3} \\ &= -\frac{\Lambda_x T}{4\pi v_x v_y} \sum_{m>0} \frac{\omega_m}{(\omega_m^2 + \Lambda_x^2)^2} \approx -\frac{1}{16\pi^2 v_x v_y} \frac{\Lambda_x}{\Lambda_x^2 + \pi^2 T^2}. \end{aligned} \quad (\text{A6})$$

$$I_{1212} \Big|_2 \approx -\frac{T \Lambda_x}{2\pi^2 v_x v_y} \sum_m \int_{\Lambda_y}^{\infty} dy \frac{1}{(y^2 + \omega^2)^2} \approx -\frac{1}{16\pi^2 v_x v_y} \frac{\Lambda_x}{\Lambda_y^2}. \quad (\text{A7})$$

Since $\Lambda_y \gg \Lambda_x$, we can ignore the second contribution and $I_{1212} \approx I_{1212}|_1$. Note that we have made the approximation $T \sum_{m>0} F(\omega_m) \approx \int_{\pi T}^{\infty} \frac{d\omega}{2\pi} F(\omega)$.

Similarly, we have the following contributions to w_a ,

$$I_{2565} = -T \sum_m \int_{|k| < \Lambda} \frac{1}{(i\omega_m + v_x k_x + v_y k_y)^2} \frac{1}{(i\omega_m - v_x k_x + v_y k_y)} \frac{1}{(i\omega_m + v_x k_x - v_y k_y)}, \quad (\text{A8})$$

$$I_{1256} = -T \sum_m \int_{|k| < \Lambda} \frac{1}{(i\omega_m - v_x k_x - v_y k_y)} \frac{1}{(i\omega_m - v_x k_x + v_y k_y)} \frac{1}{(i\omega_m + v_x k_x + v_y k_y)} \frac{1}{(i\omega_m + v_x k_x - v_y k_y)}. \quad (\text{A9})$$

Then,

$$I_{2565} = -\frac{T}{4\pi^2 v_x v_y} \sum_m \int_{-\Lambda_x}^{\Lambda_x} dx \int_{-\Lambda_y}^{\Lambda_y} dy \frac{1}{(i\omega_m + x + y)^2} \frac{1}{(i\omega_m - x + y)} \frac{1}{(i\omega_m + x - y)}, \quad (\text{A10})$$

$$I_{2565} \Big|_1 = \frac{T}{16\pi v_x v_y} \sum_m \int_{-\Lambda_x}^{\Lambda_x} dx \frac{\text{sgn}(\omega_m)}{\omega_m} \frac{1}{(x + i\omega_m)^2} \approx -\frac{1}{8\pi^2 v_x v_y \Lambda_x} \ln \left(\frac{\Lambda_x}{\pi T} \right), \quad (\text{A11})$$

$$I_{2565} \Big|_2 \approx \frac{\Lambda_x T}{2\pi^2 v_x v_y} \sum_m \int_{|y| > \Lambda_y} \frac{1}{(i\omega_m + y)^2} \frac{1}{y^2 + \omega_m^2} \approx \frac{\Lambda_x}{4\pi^3 v_x v_y} \int_{-\infty}^{\infty} d\omega \int_{\Lambda_y}^{\infty} dy \frac{2(y^2 - \omega^2)}{(y^2 + \omega^2)^3}, \quad (\text{A12})$$

$$I_{2565} \Big|_2 \approx \frac{1}{16\pi^2 v_x v_y} \frac{\Lambda_x}{\Lambda_y^2}. \quad (\text{A13})$$

Therefore, we can approximate $I_{2565} \approx I_{2565}|_1$. Similarly, we have

$$I_{1256} = -\frac{T}{4\pi^2 v_x v_y} \sum_m \int_{-\Lambda_x}^{\Lambda_x} dx \int_{-\Lambda_y}^{\Lambda_y} dy \frac{1}{(i\omega_m - x - y)} \frac{1}{(i\omega_m - x + y)} \frac{1}{(i\omega_m + x + y)} \frac{1}{(i\omega_m + x - y)}, \quad (\text{A14})$$

$$I_{1256} \Big|_1 = -\frac{T}{8\pi v_x v_y} \sum_m \int_{-\Lambda_x}^{\Lambda_x} dx \frac{\text{sgn}(\omega_m)}{\omega_m} \frac{1}{\omega_m^2 + x^2}. \quad (\text{A15})$$

The above integral is convergent in the limit of $\Lambda_x \rightarrow \infty$ (and the singularity comes from small momenta), so that

$$I_{1256} \Big|_1 = -\frac{1}{4\pi^2 v_x v_y T} \sum_{m>0} \frac{1}{(2m+1)^2} = -\frac{1}{32 v_x v_y T}. \quad (\text{A16})$$

The other contribution is given by

$$I_{1256}|_2 = -\frac{T\Lambda_x}{2\pi^2 v_x v_y} \sum_m \int_{|y|>\Lambda_y} dy \frac{1}{(y^2 + \omega_m^2)^2} = -\frac{\Lambda_x}{8\pi^2 v_x v_y \Lambda_y^2}. \quad (\text{A17})$$

Let us now compute the diagram(s) contributing to u_b . They are given by

$$J_{1515} = -\frac{T}{2} \sum_m \int_{|\mathbf{k}|<\Lambda} \frac{1}{(i\omega_m - v_x k_x - v_y k_y)^2} \frac{1}{(i\omega_m + v_x k_x + v_y k_y)^2}. \quad (\text{A18})$$

This simplifies to

$$J_{1515} = -\frac{T}{8\pi^2 v_x v_y} \sum_m \int_{-\Lambda_x}^{\Lambda_x} dx \int_{-\Lambda_y}^{\Lambda_y} dy \frac{1}{(i\omega_m - x - y)^2} \frac{1}{(i\omega_m + x + y)^2}, \quad (\text{A19})$$

$$J_{1515}|_1 = -\frac{T\Lambda_x}{8\pi v_x v_y} \sum_m \frac{\text{sgn}(\omega_m)}{\omega_m^3}, \quad (\text{A20})$$

$$J_{1515}|_1 = -\frac{7\zeta(3)}{32\pi^4} \frac{\Lambda}{v_y T^2}. \quad (\text{A21})$$

The contribution from \mathcal{I}_2 turns out to be $J_{1515}|_2 = I_{1212}|_2$ and can therefore be ignored, compared to $J_{1515}|_1$.

We now evaluate the contribution to the terms that lead to competition between the different bond order, via the 4-point couplings, u_{ab} and \bar{u}_{ab} :

$$K_{1626} = -T \sum_m \int_{|\mathbf{k}|<\Lambda} \frac{1}{(i\omega_m + v_x k_x - v_y k_y)^2} \frac{1}{(i\omega_m - v_x k_x + v_y k_y)} \frac{1}{(i\omega_m - v_x k_x - v_y k_y)}, \quad (\text{A22})$$

$$K_{6515} = -T \sum_m \int_{|\mathbf{k}|<\Lambda} \frac{1}{(i\omega_m + v_x k_x + v_y k_y)^2} \frac{1}{(i\omega_m - v_x k_x - v_y k_y)} \frac{1}{(i\omega_m + v_x k_x - v_y k_y)}, \quad (\text{A23})$$

$$L_{2516} = -T \sum_m \int_{|\mathbf{k}|<\Lambda} \frac{1}{(i\omega_m - v_x k_x - v_y k_y)} \frac{1}{(i\omega_m - v_x k_x + v_y k_y)} \frac{1}{(i\omega_m + v_x k_x + v_y k_y)} \frac{1}{(i\omega_m + v_x k_x - v_y k_y)}. \quad (\text{A24})$$

It is straightforward to see that $K_{1626} = -M_{2515}$, $K_{6515} = -M_{1262}$, and $L_{2516} = N_{2651}(=I_{1256})$, which we evaluate in detail below.

Let us now evaluate the terms contributing to the competition terms, s_a and s_b , between CDW and SC. We start with the distinct self-energy type diagrams contributing to s_a ,

$$M_{2515} = -T \sum_m \int_{|\mathbf{k}|<\Lambda} \frac{1}{(i\omega_m + v_x k_x + v_y k_y)^2} \frac{1}{(i\omega_m - v_x k_x + v_y k_y)} \frac{1}{(-i\omega_m + v_x k_x + v_y k_y)}, \quad (\text{A25})$$

$$M_{1262} = -T \sum_m \int_{|\mathbf{k}|<\Lambda} \frac{1}{(i\omega_m - v_x k_x + v_y k_y)^2} \frac{1}{(i\omega_m - v_x k_x - v_y k_y)} \frac{1}{(-i\omega_m - v_x k_x + v_y k_y)}. \quad (\text{A26})$$

Transforming to the x, y coordinates, this becomes

$$M_{2515} = -\frac{T}{4\pi^2 v_x v_y} \sum_m \int_{-\Lambda_x}^{\Lambda_x} dx \int_{-\Lambda_y}^{\Lambda_y} dy \frac{1}{(i\omega_m + x + y)^2} \frac{1}{(i\omega_m - x + y)} \frac{1}{(-i\omega_m + x + y)}, \quad (\text{A27})$$

$$M_{1262} = -\frac{T}{4\pi^2 v_x v_y} \sum_m \int_{-\Lambda_x}^{\Lambda_x} dx \int_{-\Lambda_y}^{\Lambda_y} dy \frac{1}{(i\omega_m - x + y)^2} \frac{1}{(i\omega_m - x - y)} \frac{1}{(-i\omega_m - x + y)}. \quad (\text{A28})$$

By splitting the integral as earlier, we have from \mathcal{I}_1

$$M_{2515}|_1 = -\frac{iT}{16\pi v_x v_y} \sum_m \int_{-\Lambda_x}^{\Lambda_x} dx \frac{\text{sgn}(\omega_m)}{\omega_m^2} \frac{1}{x - i\omega_m} = \frac{T}{8\pi v_x v_y} \sum_{m>0} \int_{-\Lambda_x}^{\Lambda_x} dx \frac{1}{\omega_m(x^2 + \omega_m^2)}, \quad (\text{A29})$$

$$M_{2515}|_1 = \frac{1}{64v_x v_y T}, \quad (\text{A30})$$

where we have used the fact that $2M_{2515}|_1 = -I_{1256}|_1$. Similarly from \mathcal{I}_2 , we get

$$M_{2515} \Big|_2 \approx -\frac{T\Lambda_x}{2\pi^2 v_x v_y} \sum_m \int_{|y|>\Lambda_y} dy \frac{1}{y^2 + \omega_m^2} \frac{1}{(y + i\omega_m)^2} \approx -\frac{\Lambda_x}{4\pi^3 v_x v_y} \int_{-\infty}^{\infty} d\omega \int_{\Lambda_y}^{\infty} dy \frac{2(y^2 - \omega^2)}{(y^2 + \omega^2)^3}, \quad (\text{A31})$$

$$M_{2515} \Big|_2 \approx -\frac{\Lambda_x}{16\pi^2 v_x v_y \Lambda_y^2}. \quad (\text{A32})$$

For M_{1262} ,

$$M_{1262} \Big|_1 = -\frac{iT}{16\pi v_x v_y} \sum_m \int_{-\Lambda_x}^{\Lambda_x} dx \frac{x - 2i\omega_m}{(x - i\omega_m)^2 \omega_m^2} \text{sgn}(\omega_m) = -\frac{iT}{16\pi v_x v_y} \sum_{m>0} \int_{-\Lambda_x}^{\Lambda_x} dx \frac{4i\omega_m}{(x^2 + \omega_m^2)^2}, \quad (\text{A33})$$

$$M_{1262} \Big|_1 = \frac{1}{64v_x v_y T}, \quad (\text{A34})$$

$$M_{1262} \Big|_2 \approx \frac{T\Lambda_x}{2\pi^2 v_x v_y} \sum_m \int_{|y|>\Lambda_y} dy \frac{1}{(y^2 + \omega_m^2)^2} = \frac{\Lambda_x}{8\pi^2 v_x v_y \Lambda_y^2}. \quad (\text{A35})$$

We can ignore $M_{2515}|_2, M_{1262}|_2$ compared to $M_{2515}|_1, M_{1262}|_1$.

Let us now evaluate the only distinct vertex-correction type diagram contributing to s_a ,

$$N_{2651} = -T \sum_m \int_{|\mathbf{k}|<\Lambda} \frac{1}{(i\omega_m - v_x k_x - v_y k_y)} \frac{1}{(i\omega_m - v_x k_x + v_y k_y)} \frac{1}{(-i\omega_m - v_x k_x - v_y k_y)} \frac{1}{(-i\omega_m - v_x k_x + v_y k_y)}. \quad (\text{A36})$$

Upon transforming coordinates, we have

$$N_{2651} = -\frac{T}{4\pi^2 v_x v_y} \sum_m \int_{-\Lambda_x}^{\Lambda_x} dx \int_{-\Lambda_y}^{\Lambda_y} dy \frac{1}{(i\omega_m - x - y)} \frac{1}{(i\omega_m - x + y)} \frac{1}{(-i\omega_m - x - y)} \frac{1}{(-i\omega_m - x + y)}, \quad (\text{A37})$$

and we immediately see that $N_{2651} = I_{1256}$, as expected.

The diagrams contributing to s_b can also be evaluated analogously as follows:

$$P_{2626} = -T \sum_m \int_{|\mathbf{k}|<\Lambda} \frac{1}{(i\omega_m - v_x k_x + v_y k_y)} \frac{1}{(i\omega_m + v_x k_x - v_y k_y)^2} \frac{1}{(-i\omega_m + v_x k_x - v_y k_y)}. \quad (\text{A38})$$

However, we immediately notice that $P_{2626} = -2J_{2626} = -2J_{1515}$ (which we have already evaluated above), due to the underlying $SU(2)$ symmetry of the hot-spot theory.

Finally, let us compute the diagram contributing to the three-point function, $Y_{\mu\nu\rho}$. The one we intend to compute is

$$Y_{261} = -T \sum_m \int_{|\mathbf{k}|<\Lambda} \frac{1}{(i\omega_m - v_x k_x - v_y k_y)} \frac{1}{(i\omega_m - v_x k_x + v_y k_y)} \frac{1}{(i\omega_m + v_x k_x - v_y k_y)}, \quad (\text{A39})$$

$$Y_{261} = -\frac{T}{4\pi^2 v_x v_y} \sum_m \int_{-\Lambda_x}^{\Lambda_x} dx \int_{-\Lambda_y}^{\Lambda_y} dy \frac{1}{(i\omega_m - x - y)} \frac{1}{(i\omega_m - x + y)} \frac{1}{(i\omega_m + x - y)}. \quad (\text{A40})$$

It evaluates to

$$Y_{261} \Big|_1 = -\frac{T}{8\pi v_x v_y} \sum_m \int_{-\Lambda_x}^{\Lambda_x} dx \frac{\text{sgn}(\omega_m)}{\omega_m(x - i\omega_m)} = -\frac{T}{8\pi v_x v_y} \sum_{m>0} \int_{-\Lambda_x}^{\Lambda_x} dx \frac{2x}{\omega_m(x^2 + \omega_m^2)} = 0, \quad (\text{A41})$$

$$Y_{261} \Big|_2 = -\frac{T\Lambda_x}{2\pi^2 v_x v_y} \sum_m \int_{|y|>\Lambda_y} dy \frac{1}{(y - i\omega_m)(y^2 + \omega_m^2)} = -\frac{T\Lambda_x}{2\pi^2 v_x v_y} \sum_m \int_{\Lambda_y}^{\infty} dy \frac{2i\omega_m}{(y^2 + \omega_m^2)^2} = 0. \quad (\text{A42})$$

Therefore, we see that both pieces evaluate to zero, when working with the linearized dispersions.

APPENDIX B: FEYNMAN DIAGRAMS FOR HOT-SPOT THEORY WITH A FINITE CURVATURE

In this Appendix, we provide details for the computation of the same diagrams that were evaluated earlier, but now in the presence of a finite Fermi-surface curvature, κ . We already summarized the results in Sec. IV B.

We start with the diagrams contributing to u_a . These were already well behaved in the linearized theory in the $T \rightarrow 0$ limit, and hence should continue to be so in the presence of a finite κ . Let us evaluate them nevertheless. The distinct diagrams contributing

to u_a after performing the Matsubara summation are given by

$$\tilde{I}_{1212} = \frac{1}{8\pi^2 v_x v_y} \int_{-\Lambda_x}^{\Lambda_x} dx \int_{-\Lambda_y}^{\Lambda_y} dy \left[2 \frac{f(\varepsilon_1(x,y)) - f(\varepsilon_2(x,y))}{[\varepsilon_1(x,y) - \varepsilon_2(x,y)]^3} - \frac{f'(\varepsilon_1(x,y)) + f'(\varepsilon_2(x,y))}{[\varepsilon_1(x,y) - \varepsilon_2(x,y)]^2} \right]. \quad (\text{B1})$$

In the above, $f[\dots]$ is the Fermi-Dirac distribution function and we have changed variables to $x = v_x k_x, y = v_y k_y$. \tilde{I}_{2525} is identical in form to the above with $\varepsilon_1 \rightarrow \varepsilon_5$. We evaluate the above integrals numerically as a function of temperature for different values of κ at fixed α and vice versa. We find that \tilde{I}_{2525} identically evaluates to 0 even in the presence of a finite (but small) curvature (recall that $I_{2525} = 0$). The results for \tilde{I}_{1212} along with a comparison to the analytical predictions for I_{1212} are shown in Fig. 6(a).

Let us now move onto the diagrams contributing to w_a , which were singular ($\sim 1/T$) in our computation with the linearized dispersion. After carrying out the Matsubara summation, the distinct diagrams evaluate to

$$\begin{aligned} \tilde{I}_{2565} = & -\frac{1}{4\pi^2 v_x v_y} \int_{-\Lambda_x}^{\Lambda_x} dx \int_{-\Lambda_y}^{\Lambda_y} dy \left[\frac{1}{[\varepsilon_2(x,y) - \varepsilon_5(x,y)]^2} \left(\frac{f(\varepsilon_2(x,y))}{\varepsilon_2(x,y) - \varepsilon_6(x,y)} - \frac{f(\varepsilon_5(x,y))}{\varepsilon_5(x,y) - \varepsilon_6(x,y)} \right) \right. \\ & \left. + \frac{1}{[\varepsilon_6(x,y) - \varepsilon_5(x,y)]^2} \left(\frac{f(\varepsilon_6(x,y))}{\varepsilon_6(x,y) - \varepsilon_2(x,y)} - \frac{f(\varepsilon_5(x,y))}{\varepsilon_5(x,y) - \varepsilon_2(x,y)} \right) + \frac{f'(\varepsilon_5(x,y))}{[\varepsilon_5(x,y) - \varepsilon_2(x,y)][\varepsilon_5(x,y) - \varepsilon_6(x,y)]} \right], \quad (\text{B2}) \end{aligned}$$

$$\tilde{I}_{1256} = -\frac{1}{32\pi^2 v_x v_y} \int_{-\Lambda_x}^{\Lambda_x} dx \int_{-\Lambda_y}^{\Lambda_y} dy \left[\frac{f(\varepsilon_1(x,y)) - f(\varepsilon_5(x,y))}{xy(x+y)} - \frac{f(\varepsilon_2(x,y)) - f(\varepsilon_6(x,y))}{xy(x-y)} \right], \quad (\text{B3})$$

where we have used the explicit forms of the dispersions to simplify the expression for \tilde{I}_{1256} . We evaluate these diagrams numerically and find that both of them have a very similar behavior except at low temperatures, where \tilde{I}_{2565} is always significantly smaller than \tilde{I}_{1256} [this was the case even in our previous computation where the former went as $\sim \ln(T)$ while the latter was $\sim 1/T$]. We plot \tilde{I}_{1256} in Fig. 6(b).

Let us now compute all the terms that turned out to be $\sim 1/T^2$ in our earlier computation, which included both u_b ($|\Phi^b|^4$) and s_b ($|\Psi|^2 |\Phi^b|^2$), and study the effect of a finite κ . The diagrams that contribute to u_b are modified to

$$\tilde{J}_{1515} = \frac{1}{8\pi^2 v_x v_y} \int_{-\Lambda_x}^{\Lambda_x} dx \int_{-\Lambda_y}^{\Lambda_y} dy \left[2 \frac{f(\varepsilon_1(x,y)) - f(\varepsilon_5(x,y))}{[\varepsilon_1(x,y) - \varepsilon_5(x,y)]^3} - \frac{f'(\varepsilon_1(x,y)) + f'(\varepsilon_5(x,y))}{[\varepsilon_1(x,y) - \varepsilon_5(x,y)]^2} \right], \quad (\text{B4})$$

and $\tilde{J}_{2626} = \tilde{J}_{1515}$ even for $\kappa \neq 0$.

On the other hand, the self-energy type diagrams contributing to s_b are modified to

$$\begin{aligned} \tilde{P}_{2626} = & -\frac{1}{4\pi^2 v_x v_y} \int_{-\Lambda_x}^{\Lambda_x} dx \int_{-\Lambda_y}^{\Lambda_y} dy \left[\frac{f(\varepsilon_6(x,y)) - f(\varepsilon_2(x,y))}{[\varepsilon_6(x,y) - \varepsilon_2(x,y)][\varepsilon_6^2(x,y) - \varepsilon_2^2(x,y)]} \right. \\ & \left. + \frac{1 - 2f(\varepsilon_6(x,y))}{4\varepsilon_6^2(x,y)[\varepsilon_2(x,y) + \varepsilon_6(x,y)]} - \frac{f'(\varepsilon_6(x,y))}{2\varepsilon_6(x,y)[\varepsilon_6(x,y) - \varepsilon_2(x,y)]} \right], \quad (\text{B5}) \end{aligned}$$

and $\tilde{P}_{1515} = \tilde{P}_{2626}$, even when $\kappa \neq 0$. Similarly, the vertex-correction diagrams are modified to

$$\tilde{Q}_{2626} = -\frac{1}{8\pi^2 v_x v_y} \int_{-\Lambda_x}^{\Lambda_x} dx \int_{-\Lambda_y}^{\Lambda_y} dy \left[\frac{1 - 2f(\varepsilon_6(x,y))}{\varepsilon_6(x,y)} - \frac{1 - 2f(\varepsilon_2(x,y))}{\varepsilon_2(x,y)} \right] \frac{1}{\varepsilon_2^2(x,y) - \varepsilon_6^2(x,y)}, \quad (\text{B6})$$

and $\tilde{Q}_{1515} = \tilde{Q}_{2626}$. The results for \tilde{J}_{1515} , \tilde{P}_{2626} , and \tilde{Q}_{2626} are plotted in Fig. 7, along with a comparison to the respective diagrams evaluated with $\kappa = 0$. It is not surprising that the singular power-law agrees, but even the prefactor matches perfectly.

Next, we compute the diagrams contributing to s_a ($|\Psi|^2 |\Phi^a|^2$). The distinct self-energy type diagrams evaluate to

$$\begin{aligned} \tilde{M}_{1262} = & \frac{1}{4\pi^2 v_x v_y} \int_{-\Lambda_x}^{\Lambda_x} dx \int_{-\Lambda_y}^{\Lambda_y} dy \left[\frac{f(\varepsilon_1(x,y)) - f(\varepsilon_2(x,y))}{[\varepsilon_1(x,y) - \varepsilon_2(x,y)][\varepsilon_1^2(x,y) - \varepsilon_2^2(x,y)]} \right. \\ & \left. - \frac{1 - 2f(\varepsilon_2(x,y))}{4\varepsilon_2^2(x,y)[\varepsilon_2(x,y) + \varepsilon_1(x,y)]} + \frac{f'(\varepsilon_2(x,y))}{2\varepsilon_2(x,y)[\varepsilon_2(x,y) - \varepsilon_1(x,y)]} \right] \quad (\text{B7}) \end{aligned}$$

and \tilde{M}_{2515} is identical in form to the above with the replacement, $\varepsilon_1 \rightarrow \varepsilon_2$ and $\varepsilon_2 \rightarrow \varepsilon_5$. Similarly, the distinct vertex-correction type diagrams evaluate to

$$\tilde{N}_{2615} = -\frac{1}{8\pi^2 v_x v_y} \int_{-\Lambda_x}^{\Lambda_x} dx \int_{-\Lambda_y}^{\Lambda_y} dy \left[\frac{1 - 2f(\varepsilon_2(x,y))}{\varepsilon_2(x,y)} - \frac{1 - 2f(\varepsilon_5(x,y))}{\varepsilon_5(x,y)} \right] \frac{1}{\varepsilon_5^2(x,y) - \varepsilon_2^2(x,y)}, \quad (\text{B8})$$

and where \tilde{N}_{2651} can be obtained from the above by replacing $\varepsilon_5 \rightarrow \varepsilon_1$. The results are plotted in Fig. 8.

Finally, let us evaluate the three-point functions, t_{ab} . Recall that in the linearized theory, this was identically 0. In the presence of a curvature, it is modified to

$$\begin{aligned} \tilde{Y}_{261} = & -\frac{1}{4\pi^2 v_x v_y} \int_{-\Lambda_x}^{\Lambda_x} dx \int_{-\Lambda_y}^{\Lambda_y} dy \left[\frac{f(\varepsilon_1(x,y))}{[\varepsilon_1(x,y) - \varepsilon_2(x,y)][\varepsilon_1(x,y) - \varepsilon_6(x,y)]} \right. \\ & \left. + \frac{1}{\varepsilon_2(x,y) - \varepsilon_6(x,y)} \left(\frac{f(\varepsilon_2(x,y))}{\varepsilon_2(x,y) - \varepsilon_1(x,y)} - \frac{f(\varepsilon_6(x,y))}{\varepsilon_6(x,y) - \varepsilon_1(x,y)} \right) \right], \end{aligned} \quad (\text{B9})$$

and where \tilde{Y}_{261} is still equal to the other symmetry-related diagrams. The results for \tilde{Y}_{261}/κ and $\alpha\tilde{Y}_{261}$ are shown in Figs. 9(a) and 9(b), respectively, along with a comparison to the particular form, \mathcal{Y} , that we guessed.

-
- [1] A. Damascelli, Z. Hussain, and Z.-X. Shen, *Rev. Mod. Phys.* **75**, 473 (2003).
- [2] A. Kanigel *et al.*, *Nat. Phys.* **2**, 447 (2006); T. Kondo, A. D. Palczewski, Y. Hamaya, T. Takeuchi, J. S. Wen, Z. J. Xu, G. Gu, and A. Kaminski, *Phys. Rev. Lett.* **111**, 157003 (2013).
- [3] Kai-Yu Yang, T. M. Rice, and Fu-Chun Zhang, *Phys. Rev. B* **73**, 174501 (2006).
- [4] Jia-Wei Mei, Shinji Kawasaki, Guo-Qing Zheng, Zheng-Yu Weng, and Xiao-Gang Wen, *Phys. Rev. B* **85**, 134519 (2012).
- [5] M. Punk and S. Sachdev, *Phys. Rev. B* **85**, 195123 (2012).
- [6] D. Chowdhury and S. Sachdev, [arXiv:1409.5430](https://arxiv.org/abs/1409.5430).
- [7] L. Hayward, D. Hawthorn, R. Melko, and S. Sachdev, *Science* **343**, 1336 (2014).
- [8] A. Allais, D. Chowdhury, and S. Sachdev, [arXiv:1406.0503](https://arxiv.org/abs/1406.0503).
- [9] N. Doiron-Leyraud, C. Proust, D. LeBeouf, J. Levallois, J.-B. Bonnemaïson, R. Liang, D. A. Bonn, W. N. Hardy, and L. Taillefer, *Nature (London)* **447**, 565 (2007).
- [10] G. Ghiringelli *et al.*, *Science* **337**, 821 (2012).
- [11] A. J. Achkar *et al.*, *Phys. Rev. Lett.* **109**, 167001 (2012).
- [12] J. Chang *et al.*, *Nat. Phys.* **8**, 871 (2012).
- [13] R. Comin *et al.*, *Science* **343**, 390 (2014); E. H. da Silva Neto *et al.*, *ibid.* **343**, 393 (2014).
- [14] A. J. Achkar, F. He, R. Sutarto, J. Geck, H. Zhang, Y.-J. Kim, and D. G. Hawthorn, *Phys. Rev. Lett.* **110**, 017001 (2013).
- [15] T. Wu, H. Mayaffre, S. Kramer, M. Horvatic, C. Berthier, W. N. Hardy, R. Liang, D. A. Bonn, and M. H. Julien, *Nature (London)* **477**, 191 (2011).
- [16] T. Wu, H. Mayaffre, S. Kramer, M. Horvatic, C. Berthier, P. L. Kuhns, A. P. Reyes, R. Liang, W. N. Hardy, D. A. Bonn, and M.-H. Julien, *Nat. Commun.* **4**, 2113 (2013).
- [17] D. LeBeouf, S. Kramer, W. N. Hardy, R. Liang, D. A. Bonn, and Cyril Proust, *Nat. Phys.* **9**, 79 (2013).
- [18] J. E. Hoffman, E. W. Hudson, K. M. Lang, V. Madhavan, H. Eisaki, S. Uchida, and J. C. Davis, *Science* **295**, 466 (2002).
- [19] M. Vershinin, S. Misra, S. Ono, Y. Abe, Yoichi Ando, and A. Yazdani, *Science* **303**, 1995 (2004).
- [20] M. J. Lawler, K. Fujita, J. Lee, A. R. Schmidt, Y. Kohsaka, C. K. Kim, H. Eisaki, S. Uchida, J. C. Davis, J. P. Sethna, and Eun-Ah Kim, *Nature (London)* **466**, 347 (2010); A. Mesaros, K. Fujita, H. Eisaki, S. Uchida, J. C. Davis, S. Sachdev, J. Zaanen, M. J. Lawler, and Eun-Ah Kim, *Science* **333**, 426 (2011).
- [21] R. Comin *et al.*, [arXiv:1402.5415](https://arxiv.org/abs/1402.5415).
- [22] K. Fujita, M. H. Hamidian *et al.*, *Proc. Natl. Acad. Sci. USA* **111**, E3026 (2014).
- [23] Z. Lotfi Mahyari, A. Cannell, E. V. L. de Mello, M. Ishikado, H. Eisaki, Ruixing Liang, D. A. Bonn, and J. E. Sonier, *Phys. Rev. B* **88**, 144504 (2013).
- [24] L. Li, Y. Wang, S. Komiyama, S. Ono, Y. Ando, G. D. Gu, and N. P. Ong, *Phys. Rev. B* **81**, 054510 (2010).
- [25] I. Kokanovic, D. J. Hills, M. L. Sutherland, R. Liang, and J. R. Cooper, *Phys. Rev. B* **88**, 060505(R) (2013).
- [26] D. Haug, V. Hinkov, Y. Sidis, P. Bourges, N. B. Christensen, A. Ivanov, T. Keller, C. T. Lin, and B. Keimer, *New J. Phys.* **12**, 105006 (2010).
- [27] D. J. Scalapino, E. Loh, and J. E. Hirsch, *Phys. Rev. B* **34**, 8190 (1986).
- [28] K. Miyake, S. Schmitt-Rink, and C. M. Varma, *Phys. Rev. B* **34**, 6554 (1986).
- [29] S. Raghu, S. A. Kivelson, and D. J. Scalapino, *Phys. Rev. B* **81**, 224505 (2010).
- [30] M. Metlitski and S. Sachdev, *Phys. Rev. B* **82**, 075128 (2010).
- [31] S. Sachdev and R. LaPlaca, *Phys. Rev. Lett.* **111**, 027202 (2013).
- [32] J. Sau and S. Sachdev, *Phys. Rev. B* **89**, 075129 (2014).
- [33] J. C. Davis and D. H. Lee, *Proc. Natl. Acad. Sci. USA* **110**, 17623 (2013).
- [34] K. B. Efetov, H. Meier, and C. Pepin, *Nat. Phys.* **9**, 442 (2013).
- [35] H. Meier, C. Pepin, M. Einenkel, and K. B. Efetov, *Phys. Rev. B* **89**, 195115 (2014).
- [36] V. S. de Carvalho and H. Freire, *Ann. Phys.* **348**, 32 (2014).
- [37] A. Allais, J. Bauer, and S. Sachdev, *Phys. Rev. B* **90**, 155114 (2014).
- [38] A. Allais, J. Bauer, and S. Sachdev, *Indian J. Phys.* **88**, 905 (2014).
- [39] Y. Wang and A. Chubukov, *Phys. Rev. B* **90**, 035149 (2014).
- [40] A. Melikyan and M. R. Norman, *Phys. Rev. B* **89**, 024507 (2014).
- [41] A. M. Tsvelik and A. V. Chubukov, *Phys. Rev. B* **89**, 184515 (2014).
- [42] W. A. Atkinson, A. P. Kampf, and S. Bulut, [arXiv:1404.1335](https://arxiv.org/abs/1404.1335).
- [43] However, we do not address here the issue of how the onset temperature for CDW-a compares to the bare superconducting T_c .
- [44] P. A. Lee, *Phys. Rev. X* **4**, 031017 (2014). This paper argued that a pair-density wave state might arise due to interactions mediated by transverse components of gauge fields (that remain unscreened) in an RVB scenario by an effect analogous to the Ampere effect. We considered possible PDW states in Fig. 2(a), but they were not preferred in our computation.
- [45] P. Hosur, A. Kapitulnik, S. A. Kivelson, J. Orenstein, and S. Raghu, *Phys. Rev. B* **87**, 115116 (2013).